UNCERTAINTY OF MICROWAVE RADIATIVE TRANSFER COMPUTATIONS IN RAIN

A Dissertation

by

SUNG WOOK HONG

Submitted to the Office of Graduate Studies of
Texas A&M University
in partial fulfillment of the requirements for the degree of

DOCTOR OF PHILOSOPHY

August 2006

Major Subject: Atmospheric Sciences

UNCERTAINTY OF MICROWAVE RADIATIVE TRANSFER COMPUTATIONS IN RAIN

A Dissertation

by

SUNG WOOK HONG

Submitted to the Office of Graduate Studies of
Texas A&M University
in partial fulfillment of the requirements for the degree of

DOCTOR OF PHILOSOPHY

Approved by:

Chair of Committee,	Thomas T. Wilheit
Committee Members,	Gerald R. North
	Christian D. Kummerow
	Kai Chang
Head of Department,	Richard Orville

August 2006

Major Subject: Atmospheric Sciences

ABSTRACT

Uncertainty of Microwave Radiative Transfer Computations in Rain. (August 2006)

Sung Wook Hong,

B.S.; M.S., Seoul National University;

M.S., Texas A&M University

Chair of Advisory Committee: Dr. Thomas T. Wilheit

Currently, the effect of the vertical resolution on the brightness temperature (BT) has not been examined in depth. The uncertainty of the freezing level (FL) retrieved using two different satellites' data is large. Various radiative transfer (RT) codes yield different BTs in strong scattering conditions.

The purposes of this research were: 1) to understand the uncertainty of the BT contributed by the vertical resolution numerically and analytically; 2) to reduce the uncertainty of the FL retrieval using new thermodynamic observations; and 3) to investigate the characteristics of four different RT codes.

Firstly, a plane-parallel RT Model (RTM) of n layers in light rainfall was used for the analytical and computational derivation of the vertical resolution effect on the BT. Secondly, a new temperature profile based on observations was absorbed in the Texas A&M University (TAMU) algorithm. The Precipitation Radar (PR) and Tropical Rainfall Measuring Mission (TRMM) Microwave Imager (TMI) data were utilized for the improved FL retrieval. Thirdly, the TAMU, Eddington approximation (EDD),

Discrete Ordinate, and backward Monte Carlo codes were compared under various view angles, rain rates, FLs, frequencies, and surface properties. The uncertainty of the BT decreased as the number of layers increased. The uncertainty was due to the optical thickness rather than due to relative humidity, pressure distribution, water vapor, and temperature profile. The mean TMI FL showed a good agreement with mean bright band height. A new temperature profile reduced the uncertainty of the TMI FL by about 10%. The differences of the BTs among the four different RT codes were within 1 K at the current sensor view angle over the entire dynamic rain rate range of 10-37 GHz. The differences between the TAMU and EDD solutions were less than 0.5 K for the specular surface.

In conclusion, this research suggested the vertical resolution should be considered as a parameter in the forward model. A new temperature profile improved the TMI FL in the tropics, but the uncertainty still exists with low FL. Generally, the four RT codes agreed with each other, except at nadir, near limb or in heavy rainfall. The TAMU and the EDD codes had better agreement than other RT codes.

DEDICATION

This work is dedicated to my parents, sister, and wife who love me and whom I love.

ACKNOWLEDGEMENTS

First and foremost, thanks should be given to my advisor, Dr. Thomas T. Wilheit. His insight, help, and guidance were great through this research. I cannot fully express my gratitude to him. I would also like to thank my other committee members, Dr. Christian D. Kummerow, Dr. Gerald R. North and Dr. Kai Chang, for their helpful comments throughout this effort.

Certainly not to be forgotten are all the members of the Microwave Remote Sensing Group: Kyoung-wook Jin, for sharing his knowledge with me about the atmospheric sciences; Richard Weitz, for re-formatting the original TMI data to make it easy to use and for giving lots of comments on my programs. I am grateful for all of his efforts.

Most importantly, I would like to thank my parents (Yon-Seung Hong and In-Soon Ahn) and younger sister Ye-Sung Hong for their endless and amazing love throughout my life. Without their love, understanding, and support, I could not have completed this study.

Most special thanks should be given to my wife, Kyung-Hwa Baek, without a doubt the most astonishingly talented and beautiful woman I have ever known. She always supports me with her love. I hope this work will be a small progress toward our future dream. The author also gratefully acknowledges financial support from the NASA TRMM Program.

TABLE OF CONTENTS

Page

CHAPTER Page

LIST OF FIGURES

FIGURE Page

FIGURE Page

LIST OF TABLES

CHAPTER I

INTRODUCTION

Rainfall plays an enormous role in the dynamics of the Earth's atmosphere. Roughly three-fourths of the energy absorbed by the earth's atmosphere is derived from latent heating, which results from condensation of water vapor to form precipitation. Two-thirds of this precipitation falls in the tropical regions. Quantitative understanding of rainfall patterns and amounts is critical to determine the character of the atmosphere. Spaceborne remote sensing is the only practical approach to measuring the global-scale rainfall. Microwave radiation is minimally affected by most clouds. Accordingly, microwave radiation can be directly associated with the hydrometers themselves and thereby provide observations of rainfall.

Passive microwave rainfall estimates are usually based on microwave absorption and scattering, that is, the brightness temperatures (BT) measured with a microwave radiometer. The BT is determined by the total absorption along the view path. For channels < 23 GHz, absorption by frozen hydrometeors is small, otherwise, absorption and emission by liquid cloud drops and raindrops cause a BT increase for increasing rain rates. As the scattering effects increase, the frozen hydrometers over freezing level (FL) cause BT decrease.

This dissertation follows the style and format of the *Journal of Applied Meteorology*.

Therefore, the BT contributed by rain comes primarily from the hydrometeors below the FL (0°C isotherm) when 19 and 21 GHz channels are used to retrieve the FLs. The BTs become the important input to retrieve the interested physical properties such as FL, rainfall amount and so on.

1.1 Effects of Vertical Resolution on Brightness Temperature

The various radiative transfer (RT) codes assume different vertical resolution in their own RT Model (RTM) to compute the BT. The vertical resolution is inversely related to the number of layers in the plane-parallel atmospheric models. For the convenience of computational efficiency, small numbers of layers in the atmosphere are assumed in many RT codes. The optimal number of layer in the RTM with respect to efficiency and accuracy has not been investigated previously. In this research, the quantitative effect of the number of layers (or vertical resolution) on BTs was examined, and what number of assumed layers in the plane-parallel atmosphere is reasonable for a BT difference of less than 0.5 K as a criterion to determine the minimum range number of layers throughout the angular range using different RT codes.

1.2 Improved Freezing Level Retrieval in Oceanic Rainfall Algorithm

The FL in passive microwave rainfall retrievals determines atmospheric water vapor, and, most importantly, a rough estimate of the height of the liquid water column. Therefore, the FL is a crucial parameter in passive microwave rainfall estimations. A correct FL retrieval in passive microwave retrieval techniques is very important to

determine whether or not a rainfall retrieval algorithm is reasonable. This investigation characterized the FL differences between spaceborne radiometer-based FL and spaceborne radar-based FL, attempts to explain it on a physical basis, and proposes a fix in the operational software.

1.3 Uncertainty of Radiative Transfer Calculation among Texas A&M University, Eddington Approximation, Discrete Ordinate, and Monte Carlo Codes

In the Global Precipitation Measurement (GPM) mission, a natural outgrowth of Tropical Rainfall Measuring Mission (TRMM), there will be a variety of radiometers on the constellation satellites. Accordingly, GPM can provide various measurements in terms of frequency and other viewing parameters. For this reason, a parametric Bayesian structure is currently planned. A key element of the Bayesian structure is the uncertainty associated with each radiance used. Understanding the uncertainties associated with the RT computation for the Bayesian structure is required. There are many different RT codes to calculate the BTs under various conditions by solving the radiative transfer equation (RTE). Generally, they have different approaches for solving the scattering effects in the RTE, but the calculated BTs are utilized to retrieve the FL and the rainfall. Therefore, the discrepancy of BTs from the microwave RT codes under various conditions is useful to estimate the characteristics of each RT codes.

CHAPTER II

BACKGROUND

The radiance emitted at a wavelength λ by a blackbody with an absolute temperature T is described by the Planck function as follows:

$$B_\lambda(T) = \frac{2hc^2}{\lambda^5} \cdot \frac{1}{\exp(\frac{hc}{\lambda kT}) - 1} \tag{1}$$

where $B_\lambda(T)$ is the blackbody radiation, h is Planck's constant, k is Boltzmann's constant, and c is velocity of light. In the microwave range and at temperatures typical of the Earth, $\frac{hc}{\lambda kT}$ <<1. The Rayleigh- Jeans approximation gives $B_\lambda(T) \approx \frac{2hc^2}{\lambda^5} \cdot \frac{\lambda kT}{hc} = \frac{2ck}{\lambda^4} \cdot T$. Therefore, we can directly use the BT (T_B) instead of the radiance (B_λ) using $T_B \propto B_\lambda(T)$ in the microwave region and at typical temperatures of the Earth's atmosphere.

To measure BTs over the ocean and land, satellite-borne microwave radiometers are operating. Those BTs are the basis for estimating the FLs and rainfall in most microwave rainfall retrieval schemes which depend on the RTE.

The RTE enables satellite observations of microwave radiances to be used to estimate the FLs and rainfall.

2.1 Radiative Transfer Calculation

The radiances transferred through hydrometeors in an atmosphere are determined by the following RTE (Weinman and Davies, 1978 and Kummerow and Weinman, 1988):

$$\sin\theta\cos\phi\frac{\partial I}{\partial x}+\sin\theta\sin\phi\frac{\partial I}{\partial y}+\cos\theta\frac{\partial I}{\partial z}=-k(I-J) \tag{2}$$

where ϕ is the azimuth angle, and θ is the polar angle. k is the extinction coefficient, I is the radiance (T_B is the BT) in the θ, ϕ direction , and J is the source function.

The source function J is given as follows:

$$J[x,y,z,\theta,\phi]=(1-a)T(x,y,z)+a\int_0^{2\pi}\int_{-1}^{1}\frac{1}{4\pi}P(\theta,\phi,\theta',\phi')I(\theta',\phi')d(\cos\theta')d\phi' \tag{3}$$

where a is the albedo for single scattering, $T(x,y,z)$ is the temperature, and $P(\theta,\phi,\theta',\phi')$ is the phase function for the probability of scattering from a given direction (θ',ϕ') to a given direction (θ,ϕ).

Only the z component of (2) needs to be considered in a plane-parallel, vertically stratified atmosphere. The RTE (2) consequently becomes

$$\cos\theta\frac{dI}{dz}=-k(I-J) \tag{4}$$

The change of the BT over an infinitesimal distance ds $(=dz/\cos\theta)$ can be described using (3), (4), and BT instead of the radiance as follows:

$$\frac{dT_B}{ds}=k_aT(s)+k_s\oint P(\theta,\phi,\theta',\phi')T_B(\theta',\phi')d\Omega'-(k_a+k_s)T_B(\theta,\phi) \tag{5}$$

where $T(s)$ is the thermodynamic temperature of the layer, T_B stands for the microwave BT in the direction of the polar angle, k_a is the absorption coefficient, k_s is the scattering coefficient, and, $P(\theta,\phi,\theta',\phi')$ is the phase function, and $d\Omega$ is the solid angle.

In this case, the phase function is considered symmetric and normalized to 1 such that:

$$\oint P(\theta,\phi,\theta',\phi')d\Omega' = \oint P(\theta,\phi,\theta',\phi')d\Omega = 1 \tag{6}$$

This form (5) is mathematically equivalent to (4).

2.2 Radiative Transfer Codes

2.2.1 Texas A&M University Code

In the Texas A&M University (TAMU) code (Wilheit et al., 1994), the RTE is organized as follows:

$$\frac{dT_B}{ds} = A + S \tag{7}$$

where $A \equiv k_a \cdot \{T(s) - T_B(\theta,\phi)\}$ represents the absorption and concomitant emission, $S \equiv k_s \cdot \{\oint P(\theta,\phi,\theta',\phi')T_B(\theta',\phi')d\Omega' - T_B(\theta,\phi)\}$ represents the loss of the radiance due to scattering out of the beam and gain of the radiance due to scattering of radiance traveling in other directions being scattered into the beam with no net change in the total radiation. The TAMU code solves for the BTs by using an iterative method to integrate the RTE with this model.

2.2.2 Eddington Approximation Code

Kummerow (1993) described the Eddington approximation (EDD) code. T_B in the RTE (4) can be expanded in a series of Legendre polynomials:

$$T_B(z,\theta) = I_0(z) + I_z(z)\cos\theta + \cdots \tag{8}$$

The EDD code can be obtained if this series is truncated after first two terms. The azimuthally averaged phase function can be similarly expanded in this code:

$$P(\mu,\mu') = \frac{1}{2\pi}\int_0^{2\pi} P(\theta,\phi,\theta',\phi')d\phi = \frac{1}{2\pi}\int_0^{2\pi} P(\cos\Theta)d\phi$$

$$= 1 + 3g\mu\mu' \tag{9}$$

where $\mu = \cos\theta$ and $\mu' = \cos\theta'$, and $g = \frac{1}{2}\int_{-1}^{1} P(\mu,\mu')\mu d\mu$ is the asymmetry factor of the phase function.

The phase function $P(\theta,\phi,\theta',\phi') = P(\cos\Theta)$ is normalized such that:

$$\oint \frac{1}{4\pi} P(\theta,\phi,\theta',\phi')d\Omega' = \oint \frac{1}{4\pi} P(\theta,\phi,\theta',\phi')d\Omega = 1 \tag{10}$$

where $P(\theta,\phi,\theta',\phi')$ is 4π times larger than the phase function defined in the TAMU code.

Inserting (8) and (9) into (3) and considering symmetry in ϕ yields

$$J[z,\theta] = (1-a)T(z) + a(I_0 + g \cdot I_z \cos\theta) \tag{11}$$

Equation (4) integrated by applying $\int_0^{2\pi}\int_{-1}^{1} \frac{1}{4\pi}\cdots d(\cos\theta)d\phi$ using (5) and (7) yields

$$\frac{dI_z}{dz} = -3k(1-a)(I_0 - T(z)) \tag{12}$$

Equation (4) integrated by $\int_0^{2\pi}\int_{-1}^{1} \frac{1}{4\pi} \cdots \cos\theta \cdot d(\cos\theta) d\phi$ yields

$$\frac{dI_0}{dz} = -k(1-ag)I_z \tag{13}$$

Consequently, the diffuse radiances, I_0, in each layer can be found from

$$\frac{d^2 I_0}{dz^2} = \lambda^2 (I_0 - T(z)) \tag{14}$$

where $\lambda^2 = 3k^2(1-a)(1-ag)$.

The solution of I_0 has the form

$$I_0 = D_+ \exp(\lambda z) + D_- \exp(-\lambda z) + T(z) \tag{15}$$

where D_+ and D_- are constants to be determined from the boundary conditions of the fluxes at the top and bottom of the layer.

The source function J becomes using a linear temperature profile ($T(z) = B_0 + B_1 \cdot z$, where B_0 is surface temperature, B_1 is the lapse rate) as follows:

$$J(z,\mu) = (B_0 + \frac{3ag\mu}{2\gamma} B_1) + B_1 z + [(1 + \frac{3ag\mu}{2\gamma}) aD_+] \exp(\lambda z) + [(1 - \frac{3ag\mu}{2\gamma}) aD_-] \exp(-\lambda z) \tag{16}$$

The EDD code obtains the BTs using the constants D_+ and D_- for each layer and the boundary conditions.

2.2.3 Discrete Ordinate Code

The Eddington approximation method is an example for an approximation method for the Discrete Ordinate (DO) method. The approximation lies in the radiance vector and phase function to the first order. Therefore, only one angle is needed and radiance is decomposed into isotropic (I_0) and anisotropic (I_z) term, respectively.

In the DO method (Liou, 1992 and Stamnes et al. 1988), the scattering phase function is expanded in terms of Legendre polynomials P_l such that:

$$P(\cos\Theta) = \sum_{l=0}^{N} \varpi_l P_l(\cos\Theta) \tag{17}$$

where $\cos\Theta$ is $\mu\mu'+(1-\mu^2)^{1/2}(1-\mu'^2)^{1/2}\cos\phi$ and ϖ_l is the moment determined from the orthogonality property of Legendre polynomials as follows:

$$\varpi_l = \frac{2l+1}{2}\int_{-1}^{1} P(\cos\Theta)P_l(\cos\Theta)d\cos\Theta \tag{18}$$

From a simple calculation, $\varpi_0 = 1$ and $\varpi_1 = 3g$ can be obtained. g is the asymmetry factor. Using the additional theorem for Legendre polynomial, Equation (17) is written as

$$P(\mu,\mu') = \sum_{l=0}^{N} \varpi_l P_l(\mu)P_l(\mu') \tag{19}$$

Applying (19) and the Gaussian quadrature to (4) and (5), the DO is obtained in the form

$$\mu_i \frac{dT_{\mathbf{B}}(\tau_i,\mu_i)}{d\tau} = T(\tau_i,\mu_i) - \frac{a}{2}\sum_{l=0}^{N}\varpi_l P_l(\mu_i) \times \sum_{-j=-n}^{n} T_B(\tau_i,\mu_j)P_l(\mu_j)a_j - (1-a)T(z) \tag{20}$$

where the quadrature point $\mu_{-j} = -\mu_j, j \neq 0, i = \pm 1,...,\pm n$, and the weight $a_{-j} = a_j$ and $\sum_{j=-n}^{n} a_j = 2$.

The DO calculates the BTs using the boundary conditions and a finite difference approximation if the quadrature sets are given.

2.2.4 Monte Carlo Code

In the Monte Carlo (MC) method, virtual photons propagate through the medium based on random numbers and probability (Roberti et al., 1994). There are both forward and backward methods for the application of the MC method. The backward MC code is more time efficient, as it makes use of the reciprocity theorem, and thus has only to deal with the photons that are seen by the virtual observer. In this code, the photons are traced backward through the medium, following probabilistic interaction laws which are sampled by the selection of numbers from a quasi-random sequence. When the photon is absorbed, it contributes a BT equal to the physical temperature of the medium at that point. The net result is the average of many photons. The MC code can account for atmospheric emission, surface emission, cosmic background radiation, and multiple scattering with arbitrarily complex geometry.

The MC has three steps to calculate the BTs. The first step is to determine the distance to collision. The next step is to decide whether it is a scattering event or an absorption event. For a scattering event, the scattered direction is determined. If the photon escapes from the top of the cloud, it is absorbed of the temperature of the cosmic background. In the last step, the temperatures at which all the photons are absorbed are averaged to produce the net BT.

2.3 Atmospheric Model

A plane-parallel atmospheric model based on the TAMU RTM is selected. The TAMU RTM assumes a Marshall Palmer drop size distribution from the surface up to the FL. The lapse rate is presumed to be 6.5 K/km as in the U.S. Standard Atmosphere. The relative humidity is assumed to be 80% at the surface, and to increase linearly up to 100% at the FL. The model atmosphere is divided into 200 layers, with each being 100m thick. Figure 2.1 summarizes the TAMU RTM.

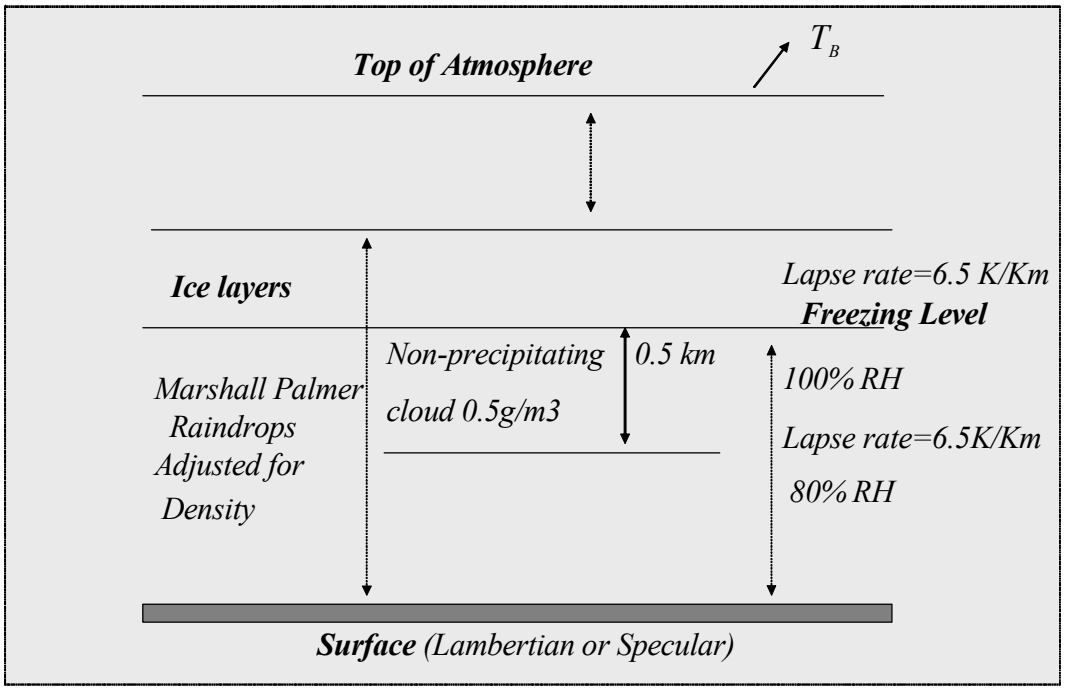

Fig. 2.1 TAMU RTM

In the TAMU RTM, the emissivity of the ocean surface is given by Fresnel relations using Lane and Saxton (1952) dielectric data. The updated oxygen and water vapor absorption models of Rosenkranz (1993, 1998) are used in this research.

The Marshall-Palmer drop size distribution is assumed in the RTM as follows:

$$N(r) = N_0 e^{-\Lambda \cdot r} \tag{21}$$

where N_0 is 0.16 cm^{-4}, Λ is $81.56R^{-0.21}$, R is the nominal rain rate in mm/hr, and r is in units of cm. The true rain rate R' is calculated by ignoring the vertical movement of the air as

$$R'(r) = \frac{4\pi}{3} \int V(r) \cdot r^3 \cdot N(r) dr \tag{22}$$

where $V(r)$ is the speed of a raindrop with radius r.

The extinction (absorption plus scattering) cross section of a dielectric sphere such as a liquid water drop (Gunn and East, 1954) is given by

$$\sigma_{ext} = -\frac{\lambda^2}{2\pi} \mathrm{Re} \sum_{n=1}^{\infty} (2n+1)(a_n + b_n) \tag{23}$$

the scattering cross section is given by

$$\sigma_{sca} = -\frac{\lambda^2}{2\pi} \sum_{n=1}^{\infty} (2n+1)(|a_n|^2 + |b_n|^2) \tag{24}$$

where a_n, b_n are the magnetic and electric 2^n pole coefficients. In the limit of a cloud droplet, and for the microwave scale, only the electric dipole term, b_1, is important. If the scattering is negligible, the extinction cross section is equivalent to the absorption cross section. In the limit of small droplets (radius less than about 100 μm) and for a

wavelength of 1.55 cm it follows that:

$$\sigma_{abs} \approx \sigma_{ext} = \frac{8\pi^2 r^3}{\lambda} \mathrm{Im}\left(\frac{k-1}{2+k}\right) \tag{25}$$

where r is the radius of the droplet, and k is the complex dielectric constant of liquid water. The absorption cross section is proportional to the volume of the droplet since $r^3 \propto volume$. This indicates that the absorption cross section is proportional to the mass of the droplet. The extinction coefficient of raindrops can be expressed as

$$\gamma_{ext} = \int N(r) \cdot \sigma_{ext} dr \tag{26}$$

where $N(r)$ is the number density of raindrops per unit volume between r and $r + dr$.

The integration of the RTE in the absence of scattering is performed from the top of the model atmosphere, with a cosmic background temperature of 2.7 °K, to the ocean surface. After that calculation, the opposite integration is calculated from the ocean surface to the top of the atmosphere. This integration procedure is common among the four RT codes. The TAMU code uses a first guess and iterates the integration of the RTE until the BT values at the top converge.

2.4 Freezing Level Retrieval Scheme Using Space-borne Microwave Sensors

The RT calculation yields different rain rate – BT (R-T) relationships for each FL and channel. In this approach, the FL acts as a proxy variable for both the rain layer thickness and the atmospheric water vapor content because R-T relationships are primarily affected by water vapor and rainfall. The combination of 19v and 21v GHz R-T relationships leads to a FLRRT (Freezing Level Rain Rate Temperature) chart to

estimate the FL .The observed BTs are used as input variables to retrieve the FL.

The TRMM satellite provides two different observational results with the PR and the TMI respectively. One is to use the BTs observed by the radiometer on the satellite. The other is to use the bright band height (BBH) caused by melting snowflakes as measured by radar on the satellite.

The basis of the Level-3 (5°x5°x1month averages) oceanic rainfall algorithms for TMI on TRMM (3A11) and AMSR-E on Aqua is given in Wilheit et al., (1991). The FLs for these algorithms are estimated by a combination of the 19.35 (18.7) and 21.3 (23.4) GHz BTs measured by TMI (AMSR-E). They are based on the close coupling between the FL and the total integrated water vapor (precipitable water) under raining conditions as reflected in the TAMU RTM (Wilheit et al., 1977). This same FL algorithm is applied in the TMI (2A12) and AMSR-E Level-2 (individual pixel) oceanic rain algorithms as well.

The FL for the PR on TRMM (2A25) algorithm is estimated by the radar returned power (reflectivity). Although snowflakes themselves above the FL have low reflectivity, their dielectric constant increases to that of water when melting. Thus, the BBH exhibits a large increase of returned power due to the thin film of water that coats the snowflakes as they melt from the outside. Below the BBH, the return signal is decreased because of the reduced size of the particles and their increased terminal velocity. Consequently, returned power is reduced. A mirror image is extremely valuable when detecting the existence of a true BBH in the returned power of PR. This is because it prevents us from misidentifying convective rain as stratiform rain. Convective rain many times appears to

have a profile similar to that of stratifom rain due to attenuation in areas of strong precipitation near the tops of the convective core. These convective cases do not display an apparent BBH in the mirror return. The presence or absence of BBH in the mirror image allows for definition and separation of stratiform and convective rain.

Only the nadir ray is used for detecting the existence of a BBH and the FL in the stratiform rain cases because only the nadir ray includes the mirror image. Comparison of the passive and the active microwave rainfall retrieval reveals that there is a discrepancy between the two. The uncertainty of retrieved FL leads in turn to uncertainty in the rainfall estimate because overestimation (underestimation) of the FL causes the underestimation (overestimation) of the rainfall.

Figure 2.2 shows an example of R-T relationships for each vertical channel from 1 to 5 km FL with 53° incidence angle. Each color represent the FLs from 1 to 5 km. Figure 2.3 shows an example of using the FLRRT chart created from Figure 2.2. The colored area in Figure 2.3 represents the occurrences of the observed BTs during December, 1999 for latitudes from +10° to -10° and longitudes from -130° to -180° when the BT of the 21 GHz channel is higher than 240 K. This sampled region is located in the tropics where the FL is relatively constant. In this example, a mean FL can be estimated as about 4.7 km over the sample area. Figure 2.4 shows a vertical profile of the returned power observed by the PR at nadir incidence on 28 Jan 1998. Figure 2.5 shows how to determine the BBH and the FL using the PR data. In this example, the FL is 4 km.

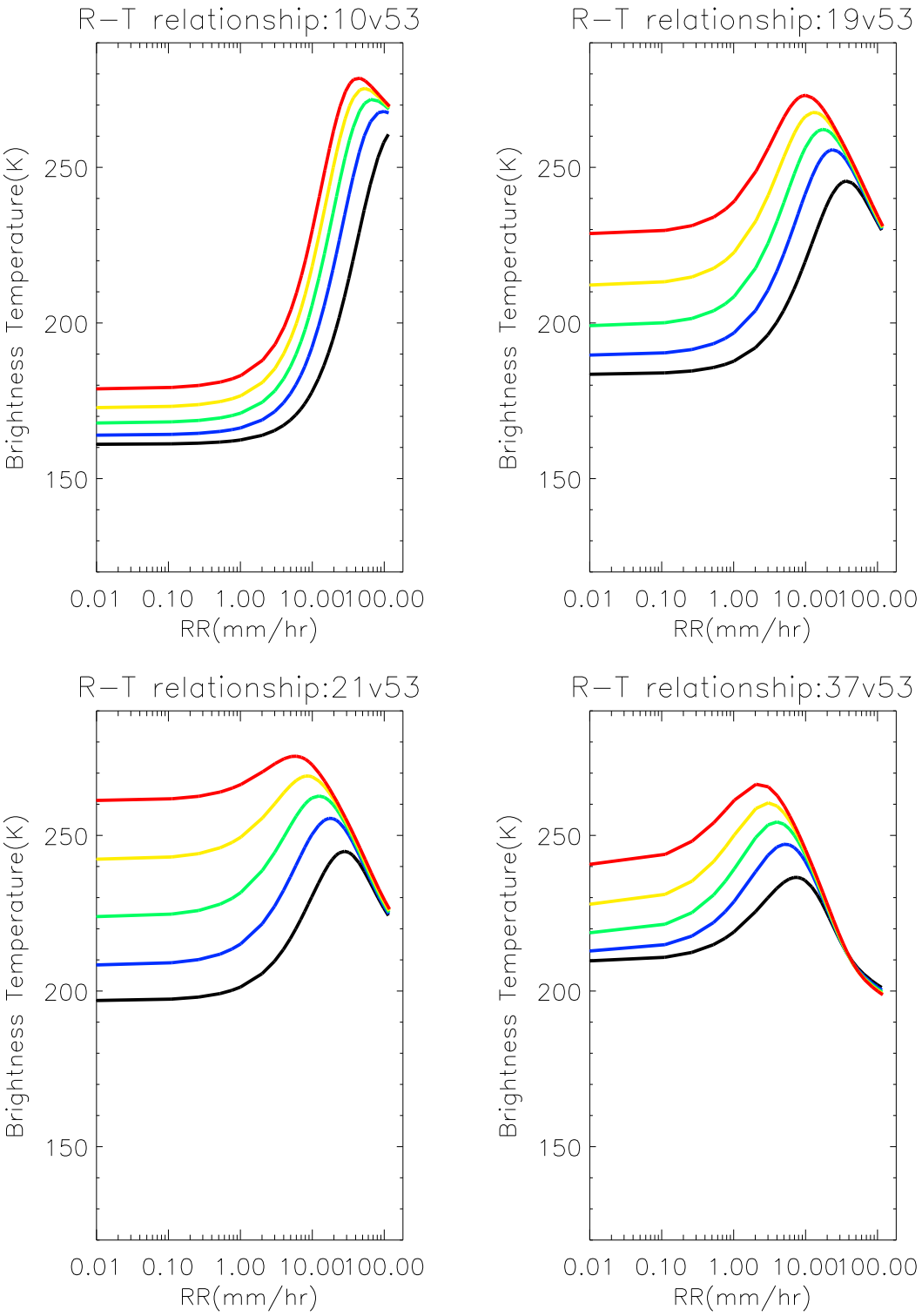

Fig 2.2 R-T relationships at 53.0° view angle using the TAMU code

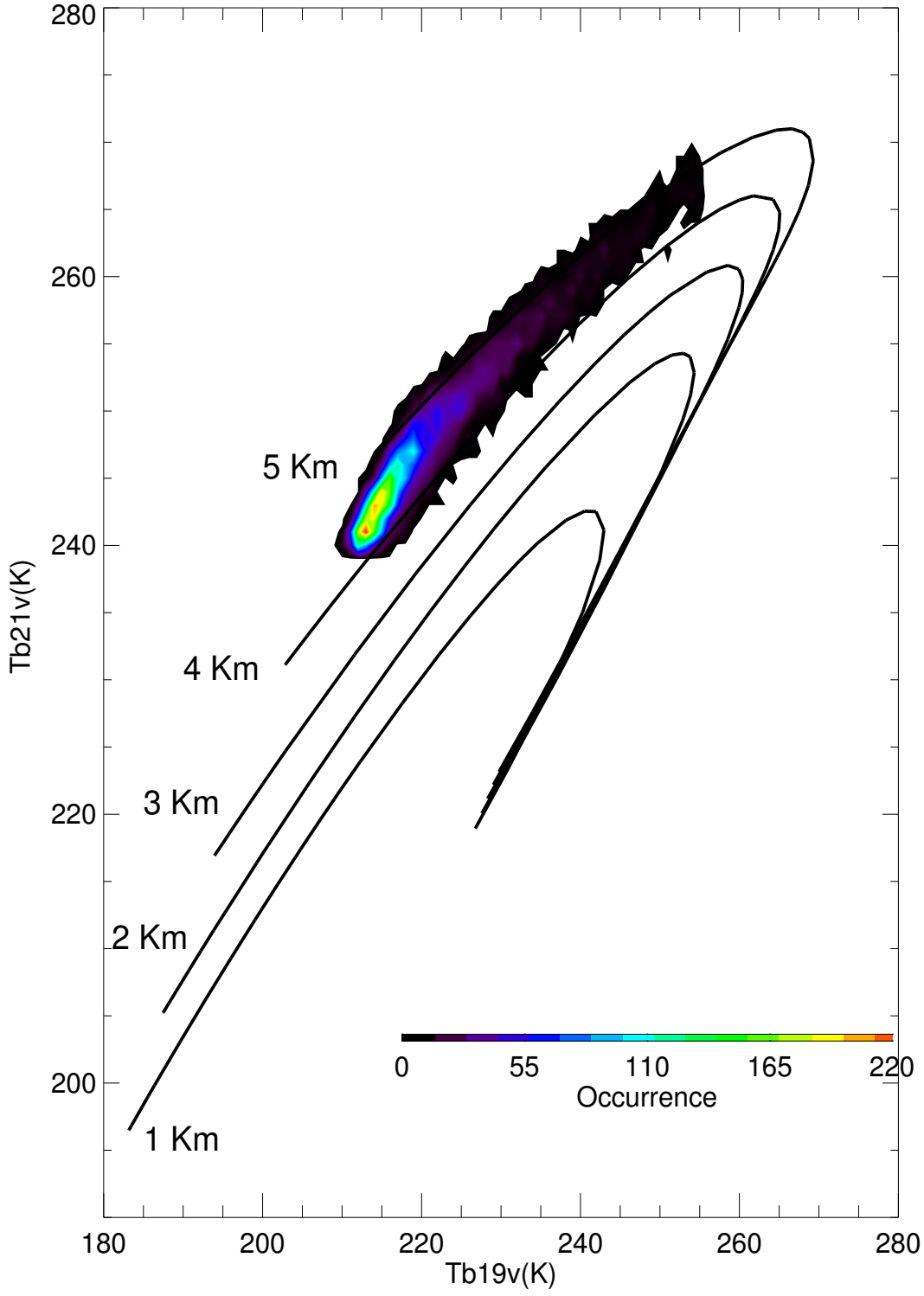

Fig. 2.3 Example of the FLRRT chart. Each curve indicates 1 to 5 km FL

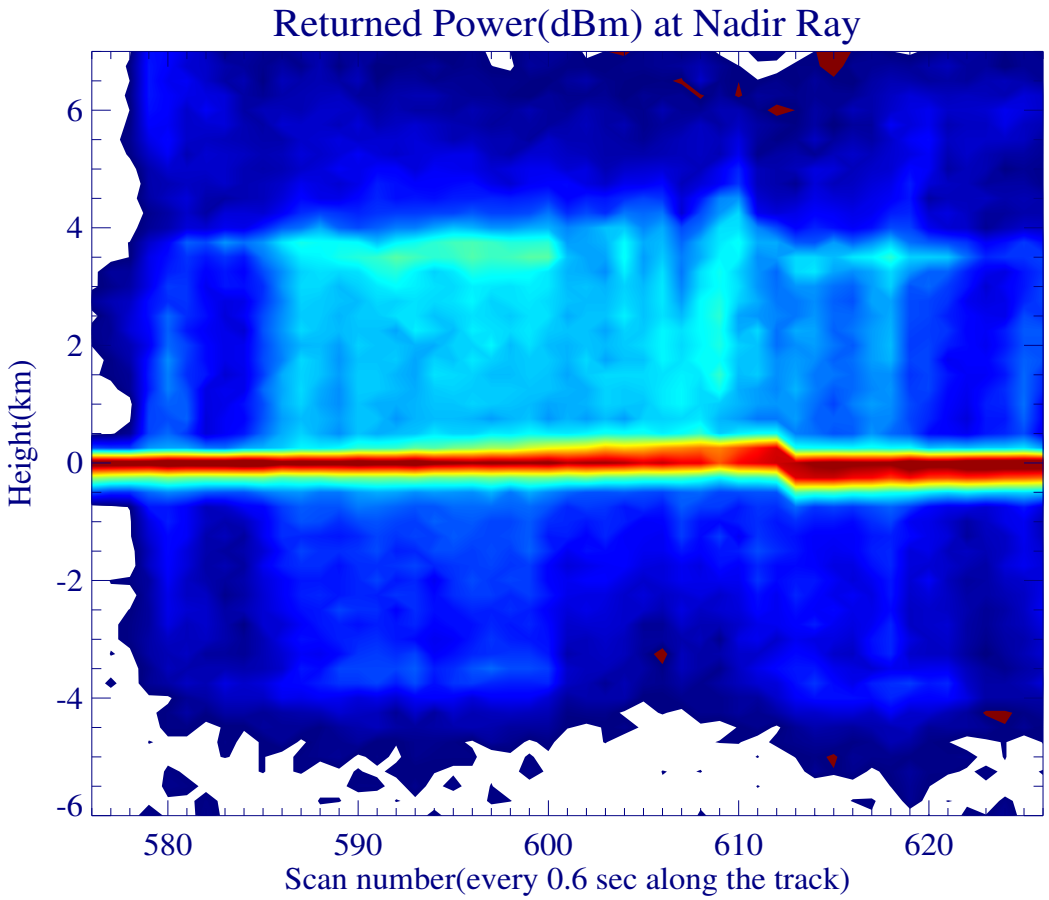

Fig 2.4 Scan of returned power (dBm) at PR nadir ray

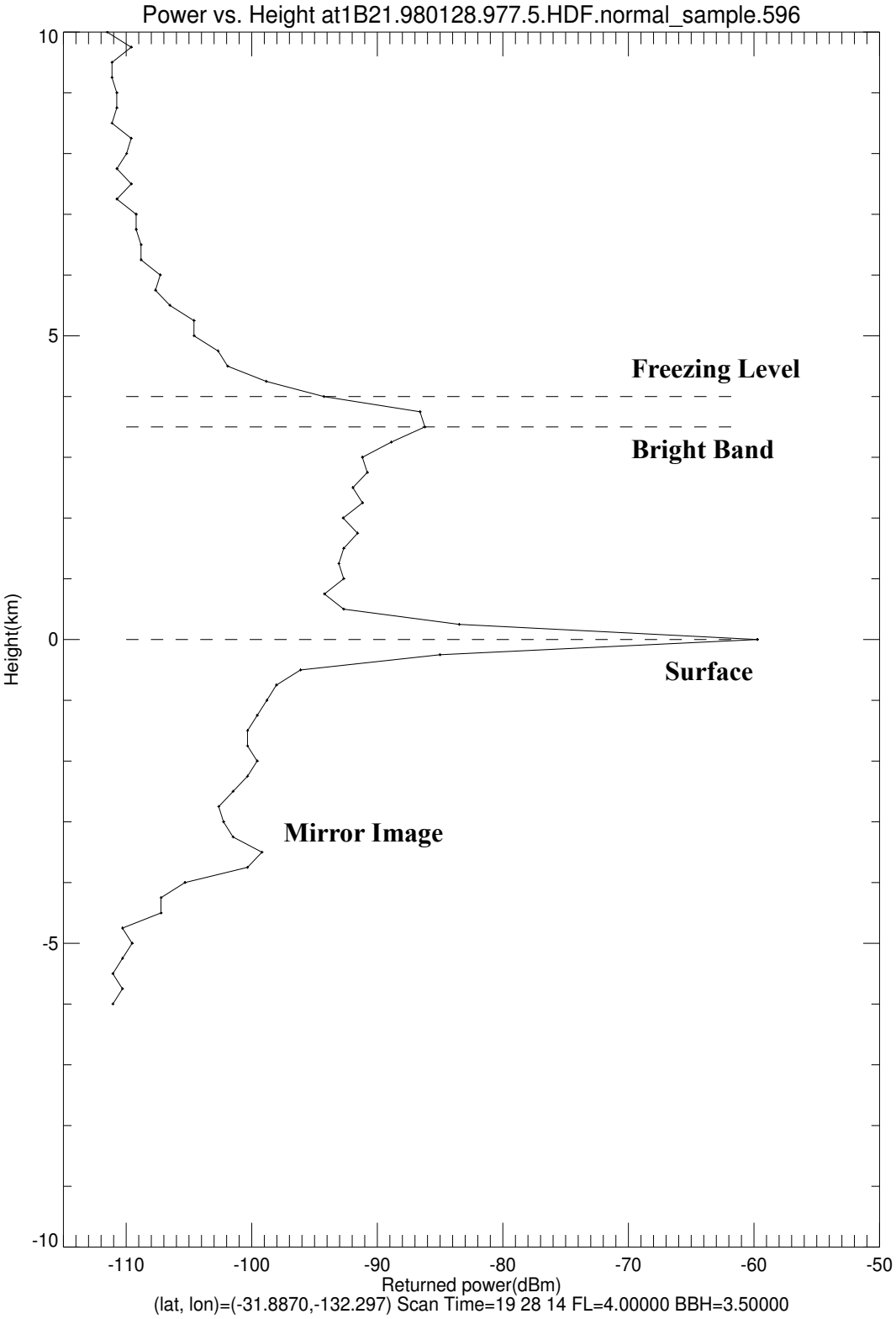

Fig. 2.5 Vertical structure of returned power. Scan number is 595

CHAPTER III

EFFECTS OF VERTICAL RESOLUTION ON BRIGHTNESS TEMPERATURE

3.1 Previous Work

Different RT codes to solve the RTE assume different numbers of layers (vertical resolution). The effect of the vertical resolution in the RTM on the BTs and the optimal number of layer in the RTM for the aspects of the efficiency and accuracy has not been investigated explicitly.

3.2 Methods

3.2.1. Analytical Derivation

a) Assumptions

For the analytical derivation of effect of vertical resolution on the BT, some assumptions are necessary. A very light rain system is considered in order to have very weak scattering. This situation enables us not to consider any particular dependency on the RT codes to calculate the differences of the BTs. Thus, the optical thickness of each layer (τ_i) is very small. Total optical thickness (τ) is almost constant independent of the number of layers.

b) Radiative Transfer Model

For the analytical derivation, a plane-parallel atmospheric model based on the TAMU

RTM is assumed to investigate the effects of number of layers on the BTs. The lapse rate (Γ) is presumed to be constant. The total thickness of atmosphere is set to Z km. The RTM is divided into n layers, with each being Z/n m thick. Each layer is numbered from 1 to n. The surface reflectivity is represented by R. Figure 3.1 summarizes the RTM for the analytical derivation.

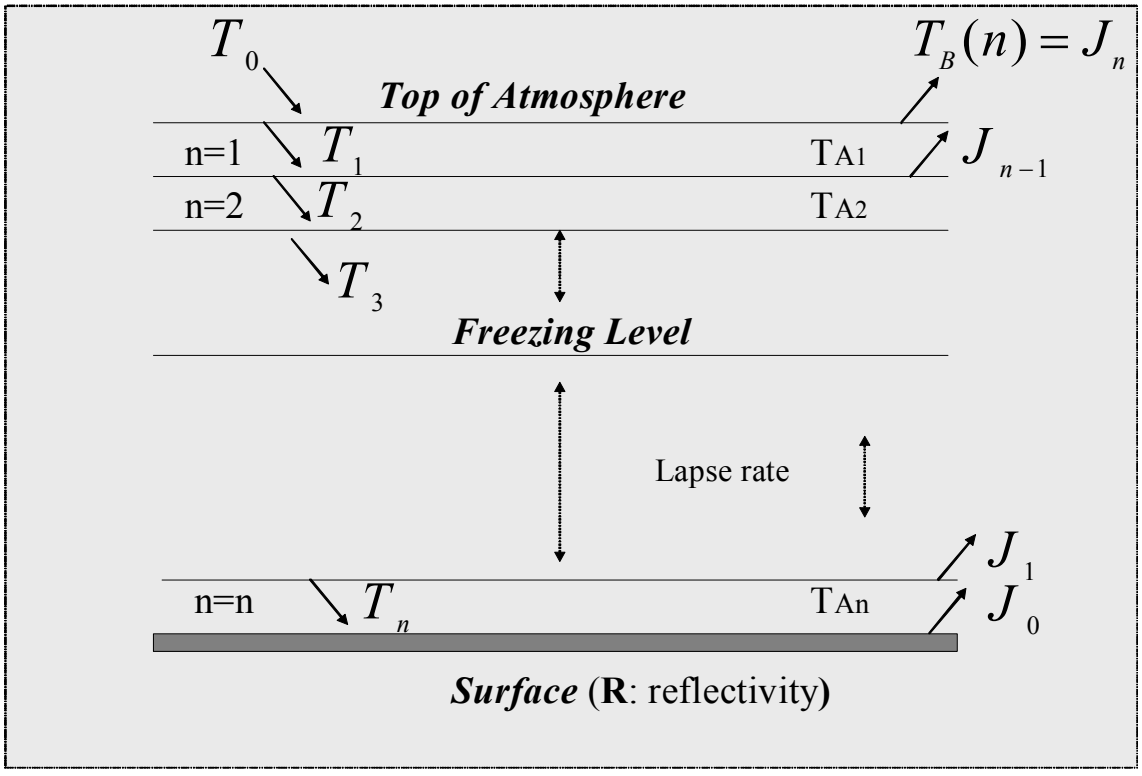

Fig. 3.1 Plane-parallel atmospheric models for the analytical derivation

c) Derivation

The transmission of layer 1 is assumed to be $e^{-\tau_1}$ and emission is assumed to be $(1 - e^{-\tau_1})$. The downwelling BT emerging from layer 1 is $T_1 = (T_0 - T_{A_1})e^{-\tau_1} + T_{A_1}$. Next step, the downwelling BT from layer 2 is

$$T_2 = (T_0 - T_{A_1})e^{-(\tau_1+\tau_2)} - (T_{A_1} - T_{A_2})e^{-\tau_2} + T_{A_1} \tag{27}$$

where

$$(T_{A_1} - T_{A_2}) = \Gamma \cdot (Z_1 - Z_2) = \Gamma \cdot \Delta Z = \Gamma \cdot \frac{Z}{n} \xrightarrow{Let} C \tag{28}$$

If the BT is consecutively calculated from the top to the surface, it is

$$T_n = (T_0 - T_{A_1})e^{-\tau} + T_{A_n} + C \cdot \Phi \tag{29}$$

where $\Phi = e^{-(\tau_2+\cdots+\tau_n)} + \cdots + e^{-(\tau_{n-1}+\tau_n)} + e^{-\tau_n}$ (30)

The BT emitted to the atmosphere from the surface is described in turn as:

$$J_0 = (T_n - T_s)R + T_s ,$$

$$J_1 = (J_0 - T_{A_1})e^{-\tau_1} + T_{A_1} ,$$

$$J_2 = (J_1 - T_{A_2})e^{-(\tau_1+\tau_2)} - (T_{A_1} - T_{A_2})e^{-\tau_1} + T_{A_1} ,$$

$$\vdots$$

Finally, the BT at the top of atmosphere becomes

$$J_n = (J_1 - T_{A_n})e^{-\tau} - C \cdot \Xi + T_{A_1} \tag{31}$$

where $\Xi = e^{-\tau_1} + e^{-(\tau_1+\tau_2)} + \cdots + e^{-(\tau_1+\tau_2+\cdots+\tau_n)}$ (32)

If the above relationships are combined, the final BT emerging at the top of the atmosphere

is obtained as follows:

$$T_B(n) = T_0 \cdot R \cdot e^{-2\tau} + (1 - R \cdot e^{-2\tau}) \cdot T_{A_1} + C_1 \cdot R \cdot [e^{-\tau} \cdot \Phi - \Xi] - C_2 \cdot (1 - R) \cdot e^{-\tau} \quad (33)$$

where $C_1 = T_{A_{i-1}} - T_{A_i} = \Gamma \cdot (\frac{Z}{n})$, (34)

$$C_2 = T_{A_n} - T_s \,, \quad (35)$$

$T_{A_1} \cdots T_{A_n}$: Temperatures of each layer (36)

3.2.2 Computational Derivation

The number of layers effect in the RT calculation is investigated using the TAMU and EDD codes. 10, 19, and 37 GHz channels are considered for this purpose. View angles from nadir to 80º in 5º increments are used. The surface is assumed to be Lambertian or specular. The FLs are assumed to be 1 or 5 km. An ice layer is also assumed even though the scattering effect is very weak For the test, number of layers are assumed to be 20, 40, 80, 100, 200, 400, and 800 layers. The analytical result is used to fit the BTs calculated from different number of layers.

a) Radiative Transfer Model

The TAMU RTM is selected to investigate the effect of number of layers. It assumes a Marshall Palmer drop size distribution from the surface up to the FL. The lapse rate is presumed to be 6.5 K/km as in the U.S. Standard Atmosphere. The relative humidity is assumed to be 80% at the surface, and to increase linearly up to 100% at the FL. The model

atmosphere is divided into n layers, with each being $20/n$ km thick. The TAMU and the EDD codes are applied to the TAMU RTM.

3.3 Results

3.3.1 Analytical Result

In order to find the effect of the number of layers (vertical resolution) on the BT, two different numbers of layers, n and $2n$, are considered for the comparison. The difference of BTs can be expressed as,

$$\begin{aligned}\Delta T &= T_B(n) - T_B(2n) \\ &= (1 - R \cdot e^{-2\tau})[T_{A_1} - T_{A_1}^{'}] + R \cdot e^{-\tau}[C_1\Phi - C^{'}_1\Phi^{'}] \\ &\quad -[C_1\Xi - C^{'}_1\Xi^{'}] - [C_2 - C^{'}_2](1-R)e^{-\tau}\end{aligned} \tag{37}$$

where

$$[T_{A_1} - T_{A_1}^{'}] = \frac{\Gamma \cdot Z}{2n}, \tag{38}$$

$$[C_1\Phi - C^{'}_1\Phi^{'}] \approx \frac{\Gamma \cdot Z}{n}[e^{-\Im} \cdot \frac{\tau}{4} - \frac{1}{2}], \tag{39}$$

$$[C_1\Xi - C^{'}_1\Xi^{'}] \approx -\frac{\Gamma \cdot Z}{n} \cdot \frac{\tau}{4}, \tag{40}$$

$$[C_2 - C_2^{'}] = -\frac{\Gamma \cdot Z}{2n} \tag{41}$$

Finally, we can obtain the effect of number of layers on the BT as follows.

$$\therefore \Delta T = \frac{1}{n} \cdot \Gamma \cdot Z \cdot [(\frac{\tau}{4} - \frac{1}{2}) \cdot R \cdot e^{-2\tau} + (\frac{1}{2} - R)e^{-\tau} + (\frac{\tau}{4} + \frac{1}{2})]$$

$$\propto \frac{1}{n} \quad (\because \cdot \Gamma, Z, R \text{ are constants, and } \tau \text{ is almost constant}) \tag{42}$$

Consequently, the uncertainty of the BT contributed by the number of layers decreases as the vertical resolution increases because the vertical resolution is inversely proportional to the number of layers.

3.3.2 Computational Result

The fitting curves using analytic result (42) ($T_B = a/n + T_0$ form, where a is sensitivity constant, T_0 is limiting temperature constant, n is the number of layers, and T_B is the BT) agree well with the BT computed from TAMU and EDD codes. As the number of layer (vertical resolution) becomes smaller, the BT difference becomes larger. The BT difference increase as the frequency becomes higher. This tendency is the same regardless of the FL.

Figure 3.2 shows the differences of BTs according to the number of layers with good agreement between analytical and computational results. The solid curves are the BT from the RT calculation for various view angles, FL, channels, and codes. The dotted curves depict the fitted results using the analytic description.

For an example of analytic derivation, we can consider a case of Γ=6.5 K/km, Z =20km, R =0.5, τ = 0.2 for 37 GHz and FL =5km, and n =100. The difference of the BT difference (ΔT) is 0.737 K in this example. This value agrees well with the computational uncertainty of the BT.

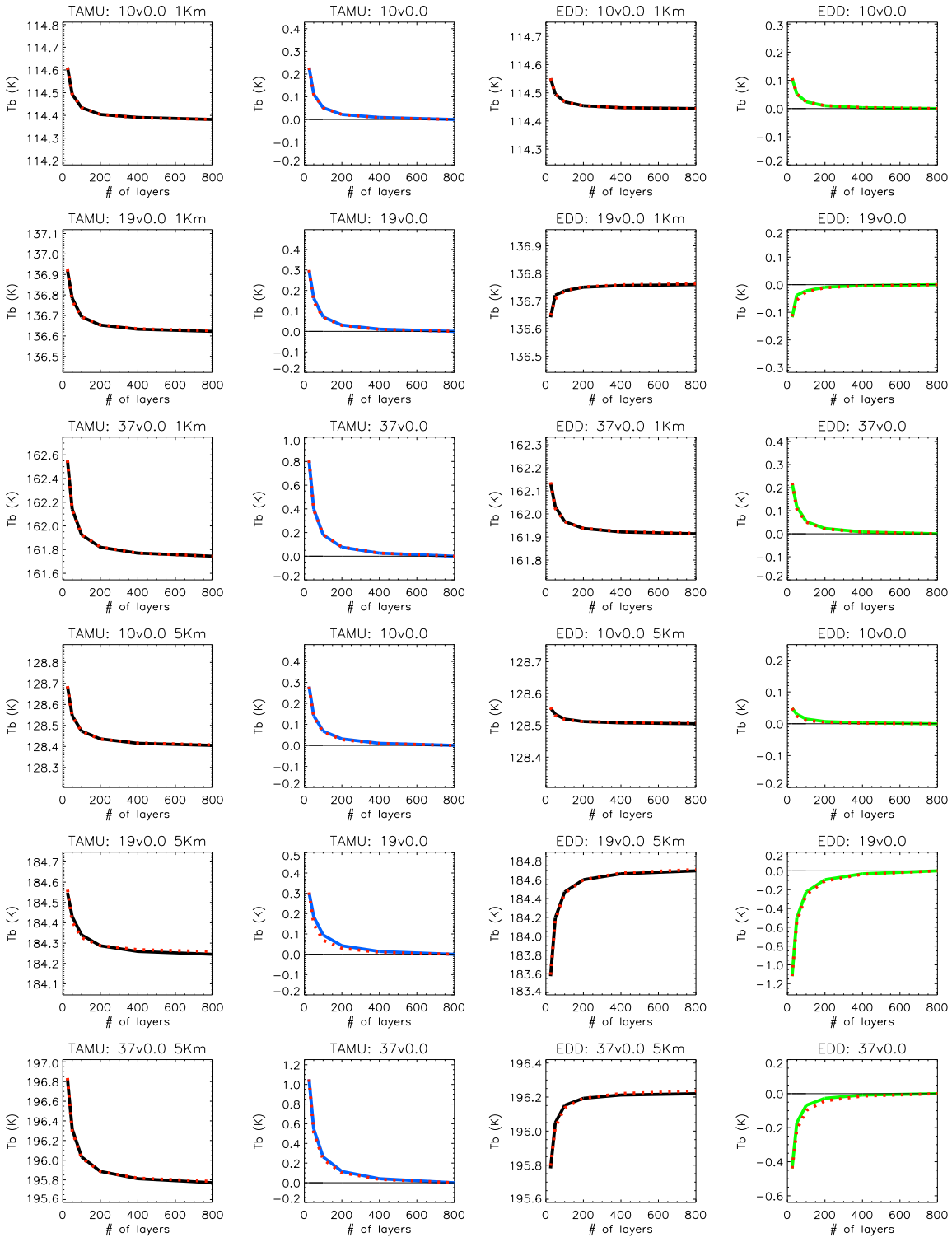

Fig. 3.2 Differences of BTs according to the number of layers from the analytical and computational results. a) Lambertian surface, FL=1 & 5 km, RR=0.001 mm/hr, View angle=nadir

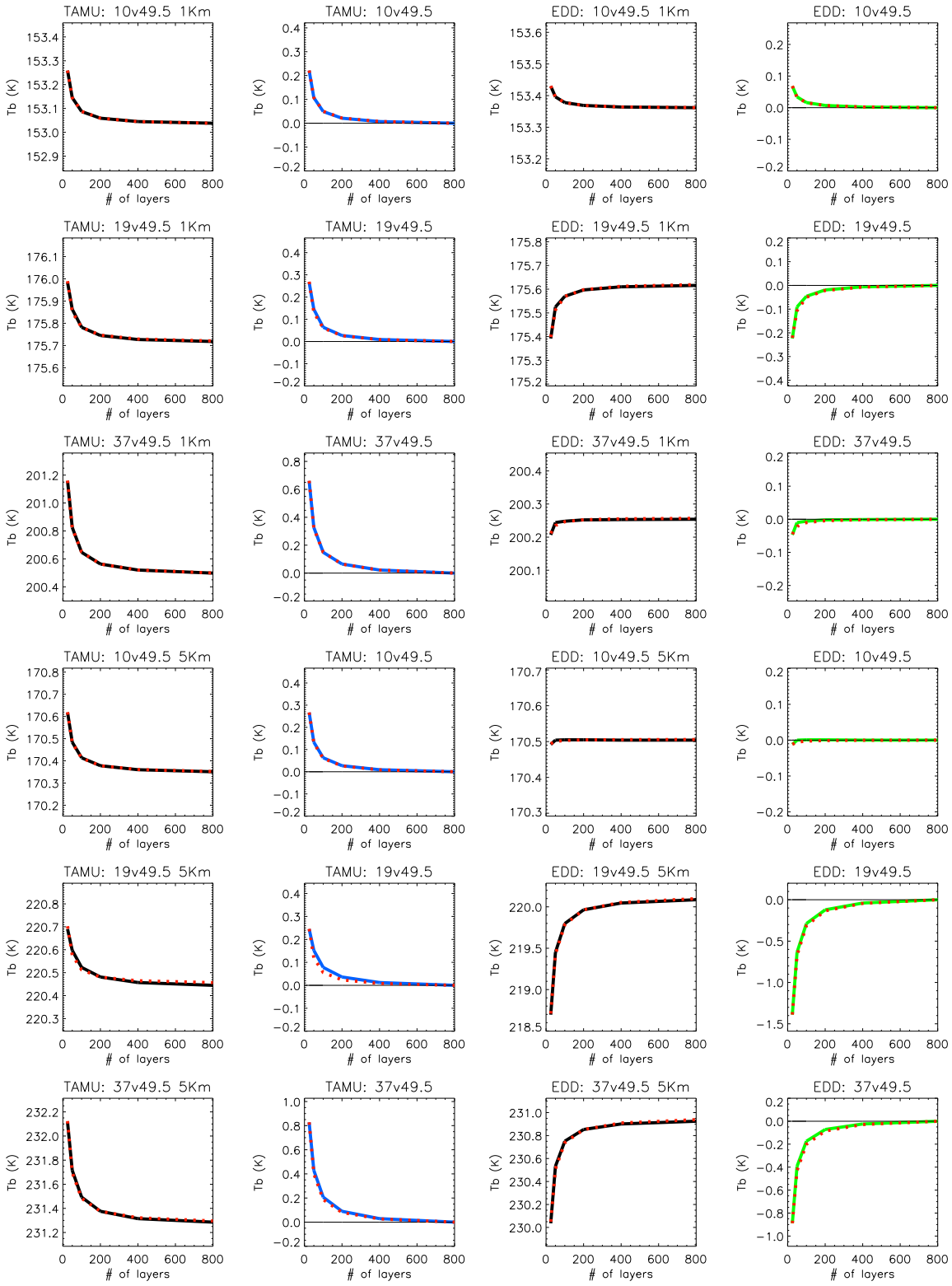

Fig. 3.2 Continued. b) Lambertian surface, FL=1 & 5km, RR=0.001 mm/hr, View angle=49.5º

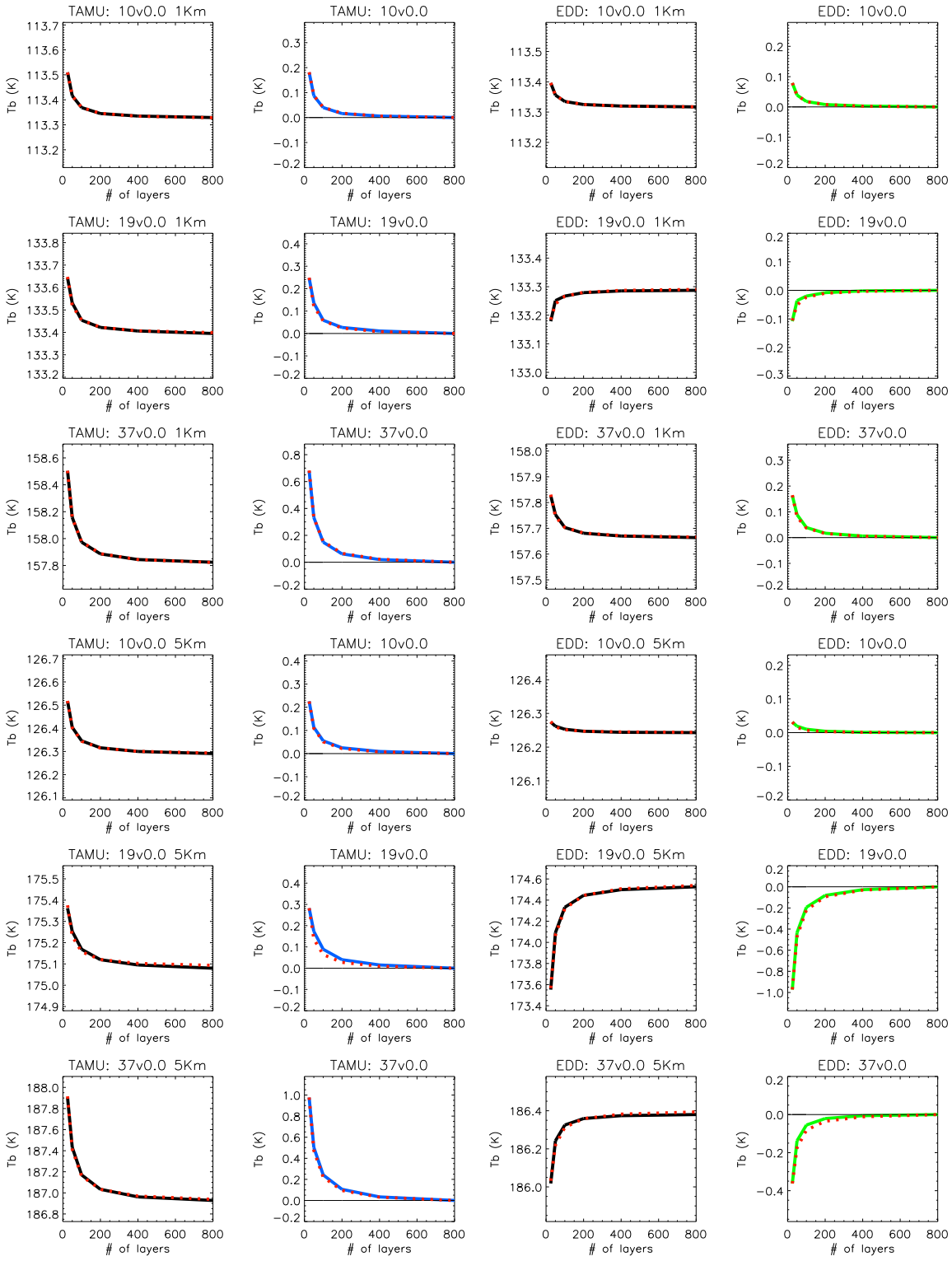

Fig. 3.2 Continued. c) Specular surface, FL=1 & 5 km, RR=0.001 mm/hr, View angle=nadir

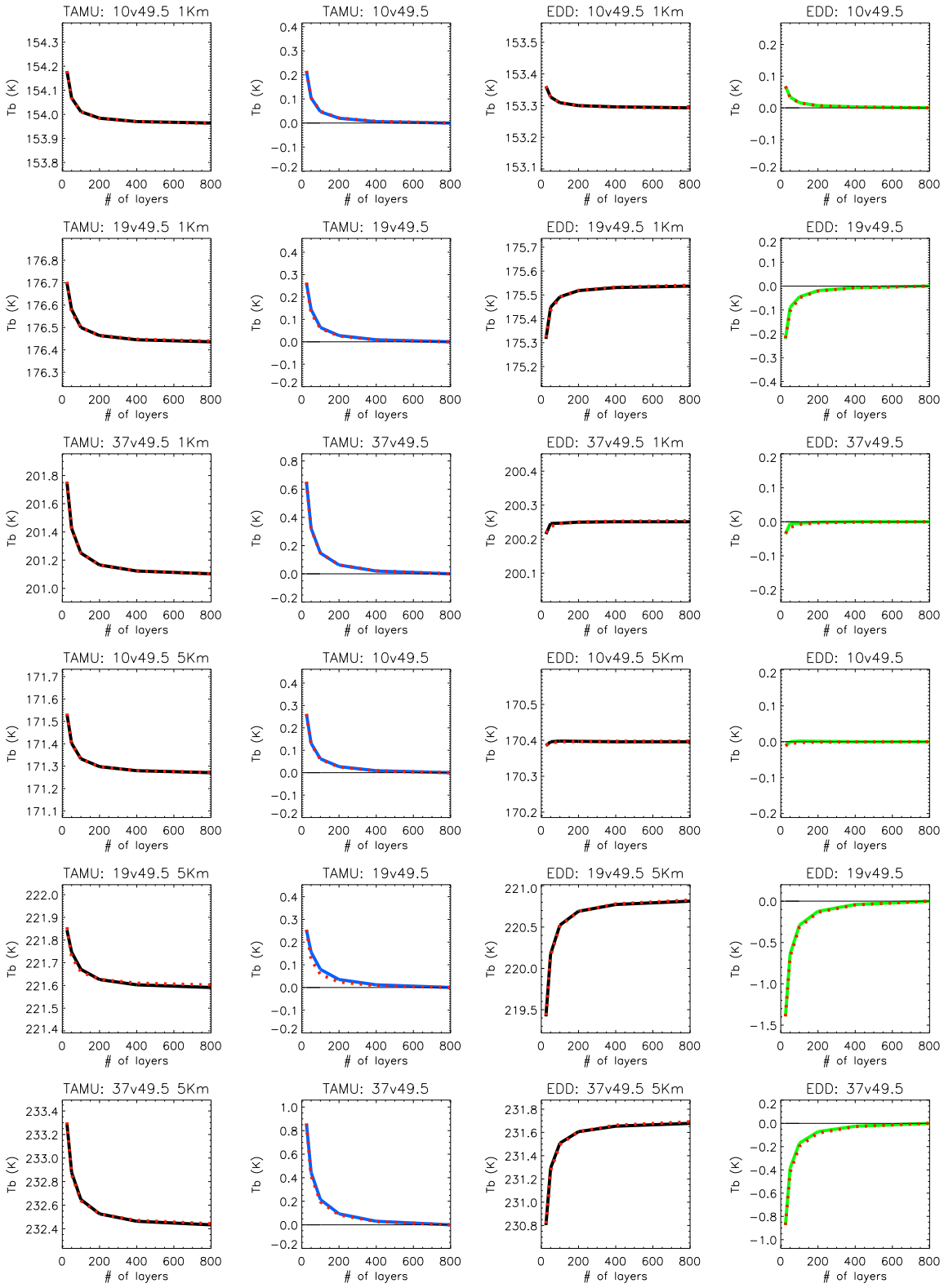

Fig. 3.2 Continued. d) Specular surface, FL=1 & 5km, RR=0.001 mm/hr, View angle=49.5º

3.3.3 Water Vapor, Temperature Profile, Relative Humidity

Water vapor, temperature profile, and relative humidity were not changed by the vertical resolution, but affected by the FL. Figure 3.3 shows the behaviors of those values for the different FLs, the different number of layers, and different surface reflections.

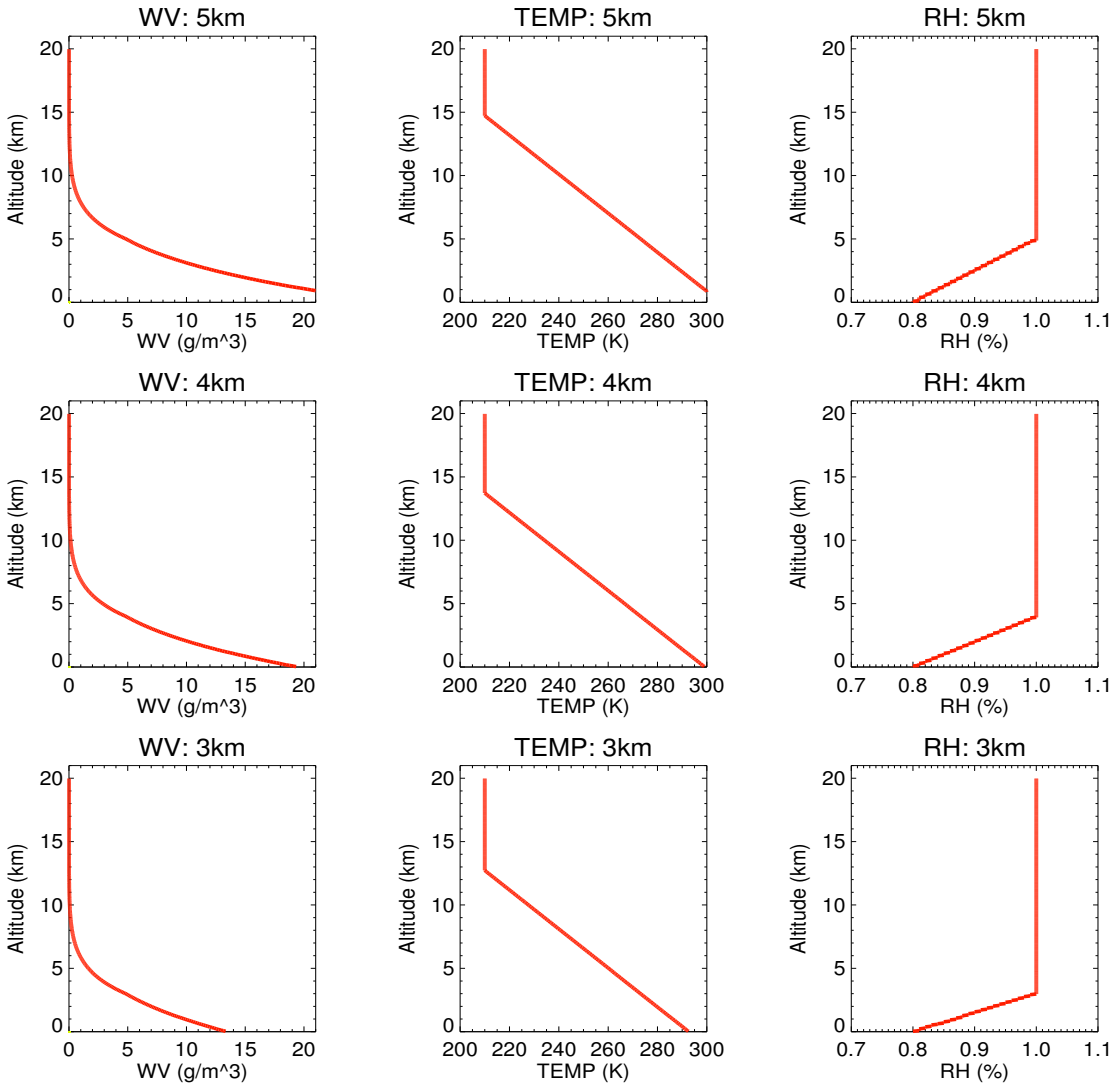

Fig. 3.3 Water vapor, temperature profile, and relative humidity for the Lambertian or specular surface with respect to the different FL from 3 to 5 km. Each color presents the different number of layers

3.3.4 Optical Thickness

The optical thickness is a function of the thickness of each layer in the RTM. Consequently, the BTs vary as a function of the number of layers in the RTM. Figures 3.4 and 3.5 show the variation of those values for the different surface properties. These values are departures from the 400 layer case. Table 3.1 describes the total optical thickness through atmospheric model for the FL from 1 to 5 km and each different number of layers. Table 3.2 summarizes the precipitable water amount for the FLs from 1 to 5 km for each number of layers.

Table 3.1 Total optical thickness through atmospheric model for the FL from 1 to 5 km and each different number of layers

FL	FQ\#of layer	20	40	80	100	200	400
5 km	10 GHz	0.024	0.024	0.024	0.024	0.024	0.024
	19 GHz	0.180	0.179	0.179	0.178	0.178	0.178
	37 GHz	0.200	0.197	0.196	0.195	0.195	0.194
4 km	10 GHz	0.019	0.019	0.019	0.019	0.019	0.019
	19 GHz	0.125	0.125	0.125	0.124	0.124	0.124
	37 GHz	0.146	0.144	0.143	0.142	0.142	0.142
3 km	10 GHz	0.016	0.016	0.016	0.016	0.016	0.016
	19 GHz	0.088	0.087	0.087	0.087	0.087	0.087
	37 GHz	0.111	0.109	0.108	0.108	0.107	0.107
2 km	10 GHz	0.014	0.014	0.014	0.014	0.014	0.014
	19 GHz	0.062	0.062	0.061	0.061	0.061	0.061
	37 GHz	0.088	0.086	0.085	0.085	0.085	0.084
1 km	10 GHz	0.013	0.013	0.013	0.013	0.013	0.013
	19 GHz	0.045	0.045	0.044	0.044	0.044	0.044
	37 GHz	0.074	0.072	0.071	0.071	0.070	0.070

Table 3.2 Precipitable water amount for the FL from 1 to 5 km and each different number of layers

FL\#of layer	20	40	80	100	200	400
5 km	7.69554	7.72257	7.72935	7.73016	7.73124	7.73153
4 km	5.18605	5.20596	5.21096	5.21155	5.21235	5.21237
3 km	3.42919	3.44362	3.44724	3.44767	3.44825	3.44839
2 km	2.22082	2.23111	2.23370	2.23400	2.23441	2.23451
1 km	1.40512	1.41234	1.41416	1.41438	1.41467	1.41473

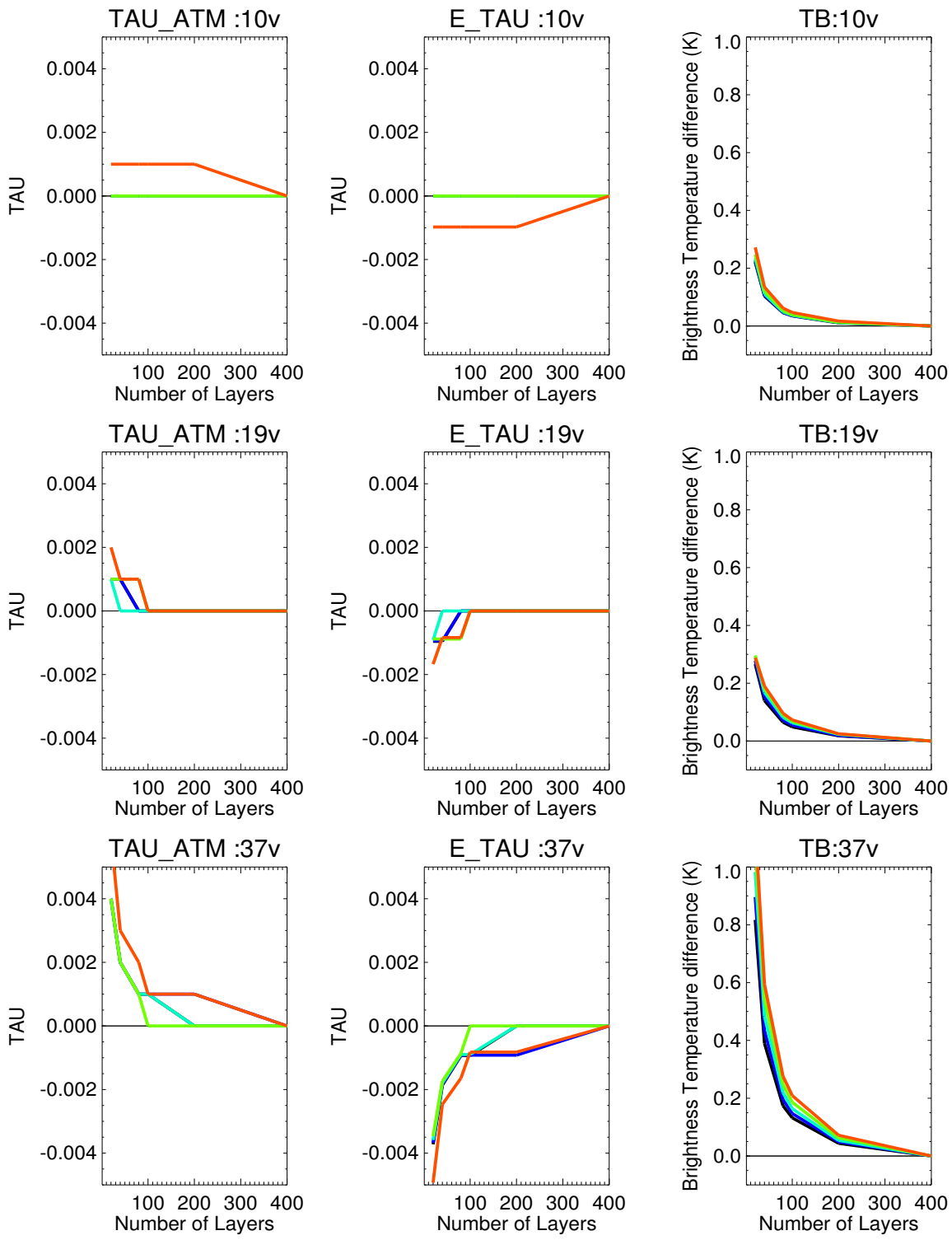

Fig. 3.4 For the specular surface, each color presents the optical thickness of atmospheric gases and absorption of the rainfall with respect to the different FL from 1 to 5 km

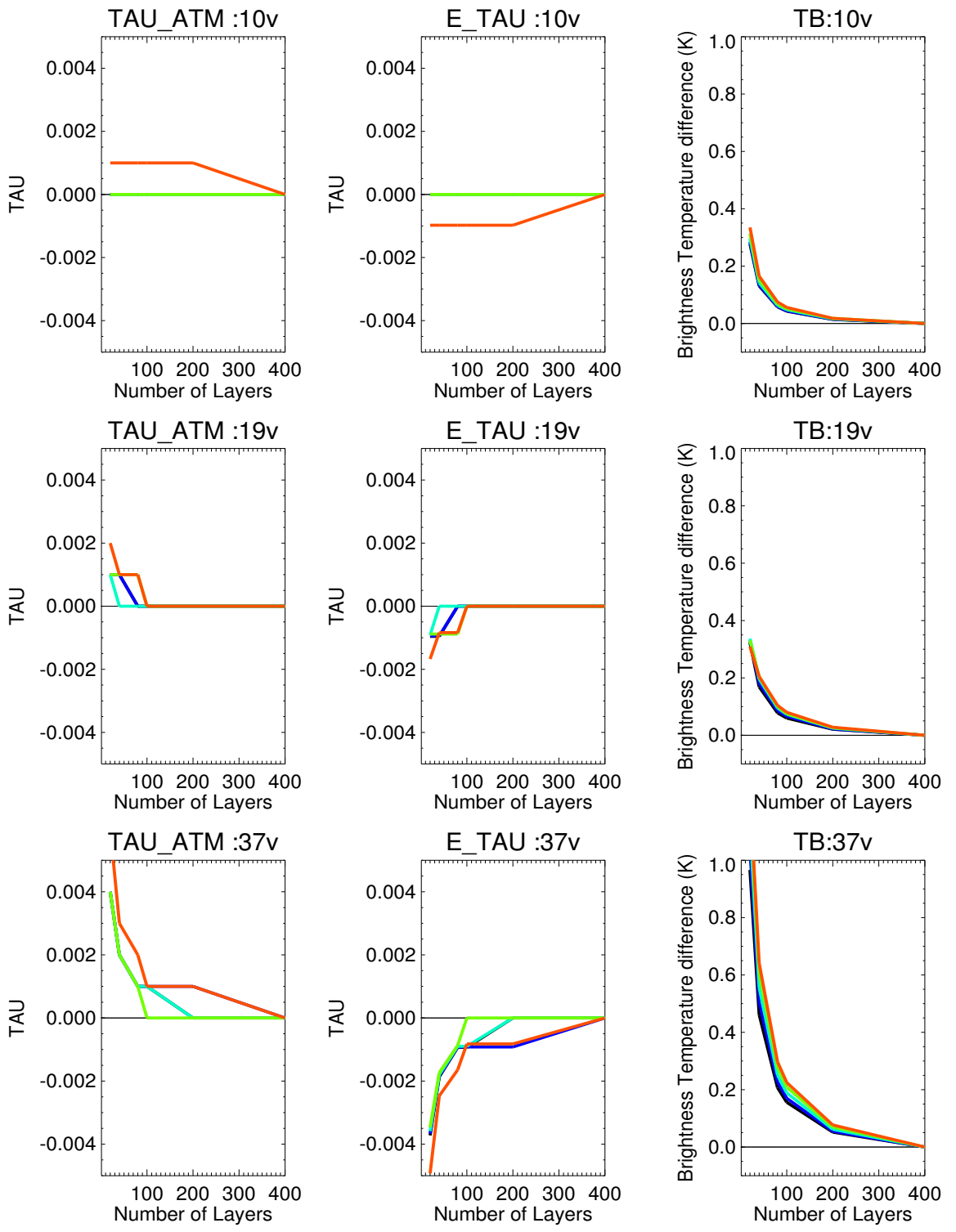

Fig. 3.5 For the Lambertian surface, each color presents the optical thickness of atmospheric gases and absorption of the rainfall with respect to the different FL from 1 to 5 km

3.3.5 Effect of Number of Layers

The good agreement between the analytic derivation and the BTs from the RTM codes can be used to investigate how many layers is most effective to balance speed versus accuracy. For this purpose, the fitted relationship was applied to the various conditions. The number of layers ranged from 1 to 200. The same TAMU RTM was assumed. To investigate the effect of number of layers, view angles from the nadir to 60° were considered to simulate the current satellite instruments. A BT difference of less than 0.5 K throughout the angular range was taken as the criterion for determining the minimum number of layers.

Figure 3.6 shows the required number of layers for the RT calculation using TAMU and EDD codes with the Lambertian and specular surface properties respectively. Each number on the figures represents the required number of layers to meet the 0.5 K criterion. Total differences of BTs were averaged from the sum of results for each frequency. For the Lambertian case, the required number of layer is approximately 44. This number of layers means the required vertical resolution is 455m. This value is roughly double of the vertical resolution of the PR. For the specular case, the required number of layers is approximately 162. This number of layers means the vertical resolution is 123m. This value is roughly half of the vertical resolution of the PR on the TRMM satellite. From these figures, the required number of layers for the specular surface assumption is larger than for the Lambertian surface case.

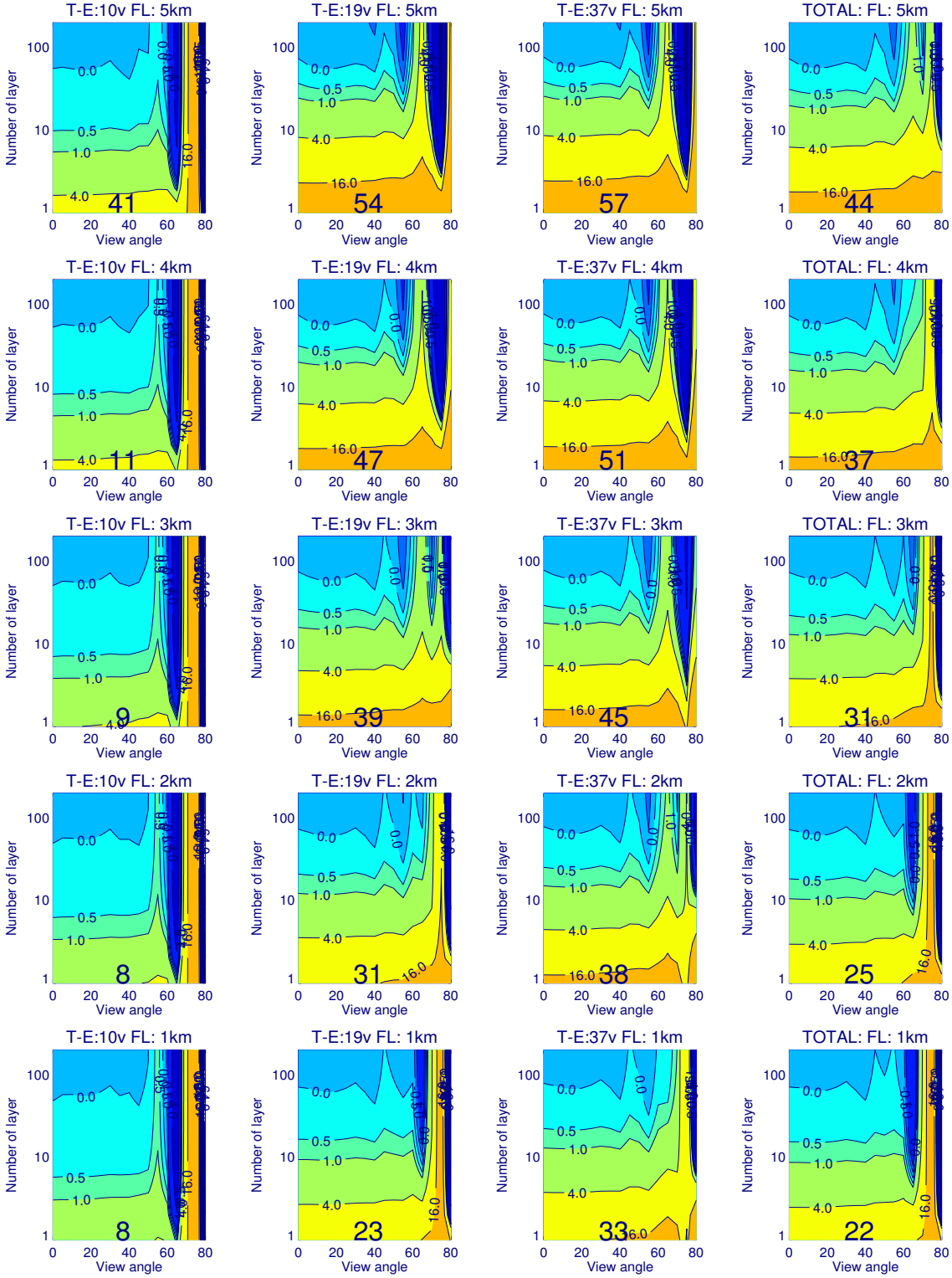

Fig 3.6 Required number of layers less than 0 K, 0.5 K, and 1 K. a) Lambertian surface case: Contour of the differences from the fitting curves for the BTs between TAMU and EDD codes

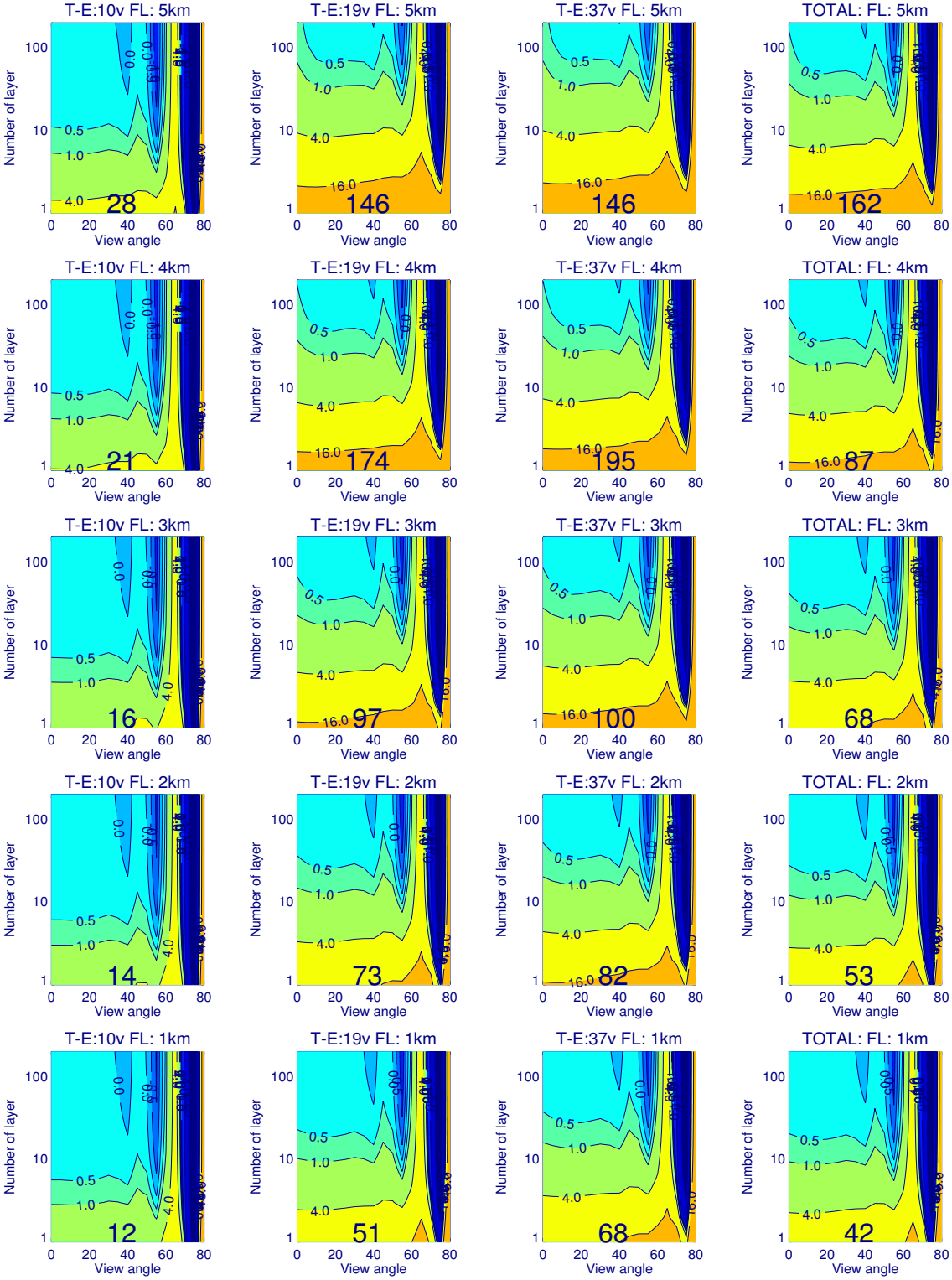

Fig 3.6 Continued. b) Specular surface case: Contour of the differences from the fitting curves for the BTs between TAMU and EDD codes

3.4 Conclusion

This research explains the effect of vertical resolution in the RT algorithm for the purpose of the computational efficiency and uncertainty through the inter-comparison among the different codes. The assumed number of layers (vertical resolution) in the passive microwave RT codes lead to slightly different BTs even if the same RTM is used. The very light rainfall case was investigated for the effect of vertical resolution on the BTs in order to have a weak scattering effect. The results of this research are very useful for understanding the internal structure of the RT algorithm to obtain the FL and rainfall retrieval although it is not applied directly to the heavy rainfall condition because the assumptions would be complicated as scattering effect increases.

The uncertainty of the BT from the vertical resolution decreases as the assumed number of layers increase; This is common to both the TAMU and EDD codes. Fewer layers are needed to obtain the same uncertainty ($\leq$ 0.5 K) for both codes for the Lambertian surface than the specular surface. Those vertical resolutions are approximately half or double the value of the PR resolution, respectively.

The uncertainties are due to the optical thickness because the layer optical thickness is a function of the vertical resolution.

This research is the first useful trial to determine the effect of vertical resolution in the RTM although the effect of number of layers is weak in the RT calculations.

CHAPTER IV

IMPROVED FREEZING LEVEL RETRIEVAL IN OCEANIC RAINFALL ALGORITHM

4.1 Previous Work

For the aspect of radar reflectivity, the FL is the height to begin the increase in reflectivity of falling particles because particles become wet and their dielectric constant becomes that of water. The BBH is the height of maximum reflectivity. Above the BBH, the particles are melting from outside. Accordingly, the reflectivity is increasing. Below the BBH, the return signal is decreasing because particle size is reducing and the terminal velocity is increasing so that it spreads the drops over a large volume. Thus, the reflectivity decreases.

Chiu and Chang (2000) showed that FLs derived from the SSM/I using a modified version of Wilheit's method compared with those estimated from a general circulation model are too high in the mid-latitude winter hemisphere. Ikai and Nakamara (2003) investigated the estimation of FL by TMI in comparison with the BBH from PR using 3-month-averaged global data. They found that the TMI-FL is higher than BBH by about 300-500 m when TMI-FL (or BBH) is high. However, when TMI-FL (or BBH) is low, this 3-month-averaged TMI-FL is higher by about 1500-2000 m than the 3-month-averaged BBH. This research implies TMI-FL is overestimated.

Thurai et al. (2003) made a comparison between the BBH obtained from the PR and the annual average of the FL available in International Telecommunications Union -

Radiometeorology Recommendation (ITU-R) P. 839-3 (Rain height model for prediction methods), which provides contours that are generated on a 1.5° by 1.5° latitude by longitude resolution grid. According to Thurai et al. (2003), the BBH typically occurs 300m below the FL. When these heights are low, additional errors occur due to the difficulty in detecting the BBH at ranges where surface echoes contribute to the radar backscatter. At present, some of the range gates below 2 km are considered as having significant clutter contamination and, for a given profile, the radar reflectivity is assumed constant below this height. When the BBH lies significantly below 2 km, the current algorithm used for the event classification will be unable to identify the event as stratiform precipitation. As a result, the estimated BBH is higher than its true value.

Previous studies show commonly that the TMI FL is reasonable in the tropics, and overestimated in the mid-latitude. Accordingly, the validated rain rates are acceptable in the tropics, and underestimated in the mid-latitude. This is related to the fact that error in the retrieved FL results, in turn, in error in the rainfall estimate because overestimation (underestimation) of the FL causes the underestimation (overestimation) of the rainfall.

4.2 Data

The primary rainfall measuring instruments on board TRMM are the TMI and the PR to measure rainfall and latent heat released through condensation in the tropical and subtropical regions.

An orbit of TRMM is defined each time the sub-satellite track reaches its southernmost latitude. The average orbit was 91.5 minutes or 5490 seconds before August

7, 2001 and 92.5 minutes or 5550s after August 24, 2001 since the orbit was adjusted during that period. The first partial orbit after launch is orbit 1, so the first full orbit is orbit 2.

A granule is defined as one orbit for PR instrument. For the TMI, a granule is defined as one orbit plus an overlap before the orbit, known as the preorbit overlap, plus an overlap after the orbit, the postorbit overlap. The overlap size is fixed at exactly 50 scans. Since the PR scans through nadir and TMI scans at a 49° angle off of nadir, collocation is needed to compare the two different measurements. The collocated measurements occur around a minute apart.

The TRMM satellite structural axes are defined so that +Z is the side where PR is mounted and is the direction normally pointed toward the nadir (straight down to the Earth). +X is the side toward which the TMI is mounted, and the side toward which the TMI takes measurements. The TRMM satellite flies with the +X axis forward half of the time, and with the –X axis forward during the other half of the time. The +Y axis is such that +X, +Y, and +Z complete a right-hand system. For TMI, scans are always left to right in the +X spacecraft direction as the microwave antenna rotates about the +Z axis. Thus TMI scans are left to right looking forward along the ground track in the +X forward mode. PR scans electronically right to left with +X forward.

4.2.1 TMI

TMI receives microwave radiation from 49° off nadir. This measured radiation can be thought of as the BT, which is related to the total amount of liquid water in the atmospheric

column. Therefore, estimates of surface rain rates are based on the height of the liquid column, namely, the freezing level. Different channels of TMI measure different BTs from the same regional position. The TMI is a microwave radiometer using five different channels (10, 19, 21, 37, and 85 GHz). Figure 4.1 shows examples of orbits of TMI BT data for each of the vertically polarized channels. The 19GHz channel responses are dominated by emission processes and respond primarily to increases in the liquid water column over oceans. So this channel is physically related to rainfall on the sea surface. The 21 GHz channel is associated with the water vapor absorption. The TMI Level-1B11, "TMI BT", is presented in a Swath Structure and formatted in HDF.

4.2.2 PR

The PR is the first precipitation radar to be used on a satellite, and operates at a frequency of 13.8GHz. The PR Level-1B21 data, which contains the received power (dBm) at the PR receiver, will be used. The PR has the complex sampling strategy. Each scan contains 49 rays sampled over an angular sector of 34°. For a given ray, the satellite begins recording samples at a fixed distance from the satellite and records a certain number of samples every 125m along the ray. The starting distance and the number of samples are different for each ray. The extra data in the nadir ray are known as the mirror image, because they record energy reflected not once from a target, but three times (surface to target to surface). Normal samples have a spacing of 250m along the ray. The mirror image is contained in the normal sample. A range bin number is defined as a distance from the satellite along the ray. It starts at 1 roughly 327km (381 km after August 24, 2001) from the

satellite, increments by 1 roughly every 250m, and increases to a maximum of 400 at roughly 377km from the satellite. The PR Level-1B21 data include the exact value for the starting distance. Retrieving the FL from PR data is based on the use of the BBH and the mirror image for stratiform rain cases. The definition of the BBH is clear, but could be subjective.

1B21 data for the PR and 1A11 data for the TMI are used from December, 1997 to January, 1998 and from December, 1999 to January, 2000. 1B21 data contain the received power at the PR receiver. 1A11 data contain TMI BTs.

4.3 Methods

4.3.1 Observations

Rangno and Hobbs (2005) investigated the microstructures and development of precipitation in cumuliform over the tropical Pacific warm pool based on in situ measurements in the TRMM/Kwajalein Experiment (KWAJEX). Their temperature measurements in rain are given in their paper. The average lapse rate is 5.26 K/km.

Berg et al. (2002) compared the structure of precipitation systems between selected east and west Pacific regions along the inter-tropical convergence zone (ITCZ) using a combination of satellite observations including vertical profile retrievals from the TRMM PR. If the lapse rate is derived from temperature profiles in their paper, it is approximately 5.3 K/km. This value is very close to the lapse rate derived from Rangno and Hobbs. (2005).

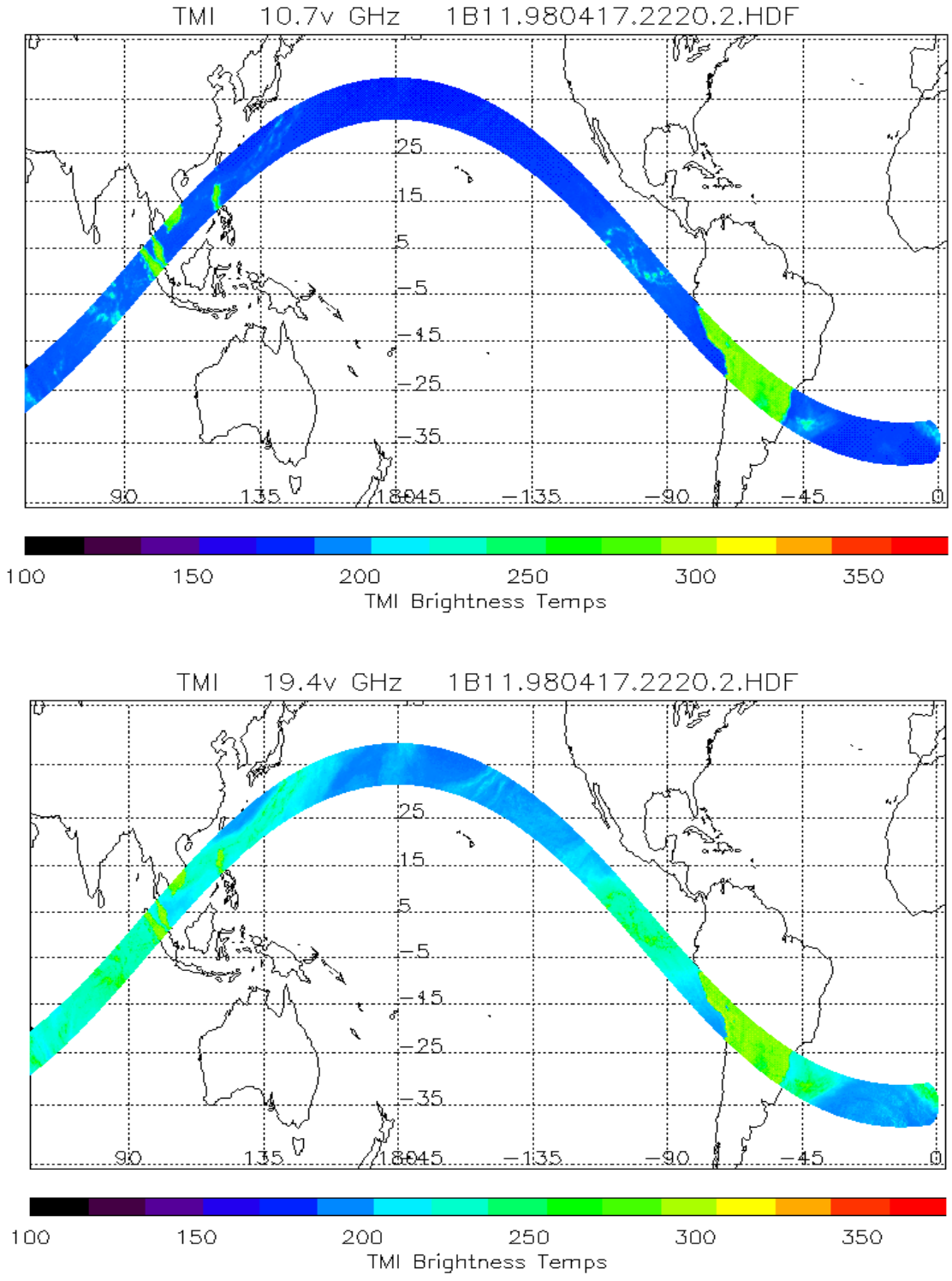

Fig. 4.1 Examples of orbit of TMI BT at 04/17/1998. a) One orbit of TMI 1B11 BT data for 10v and 19v

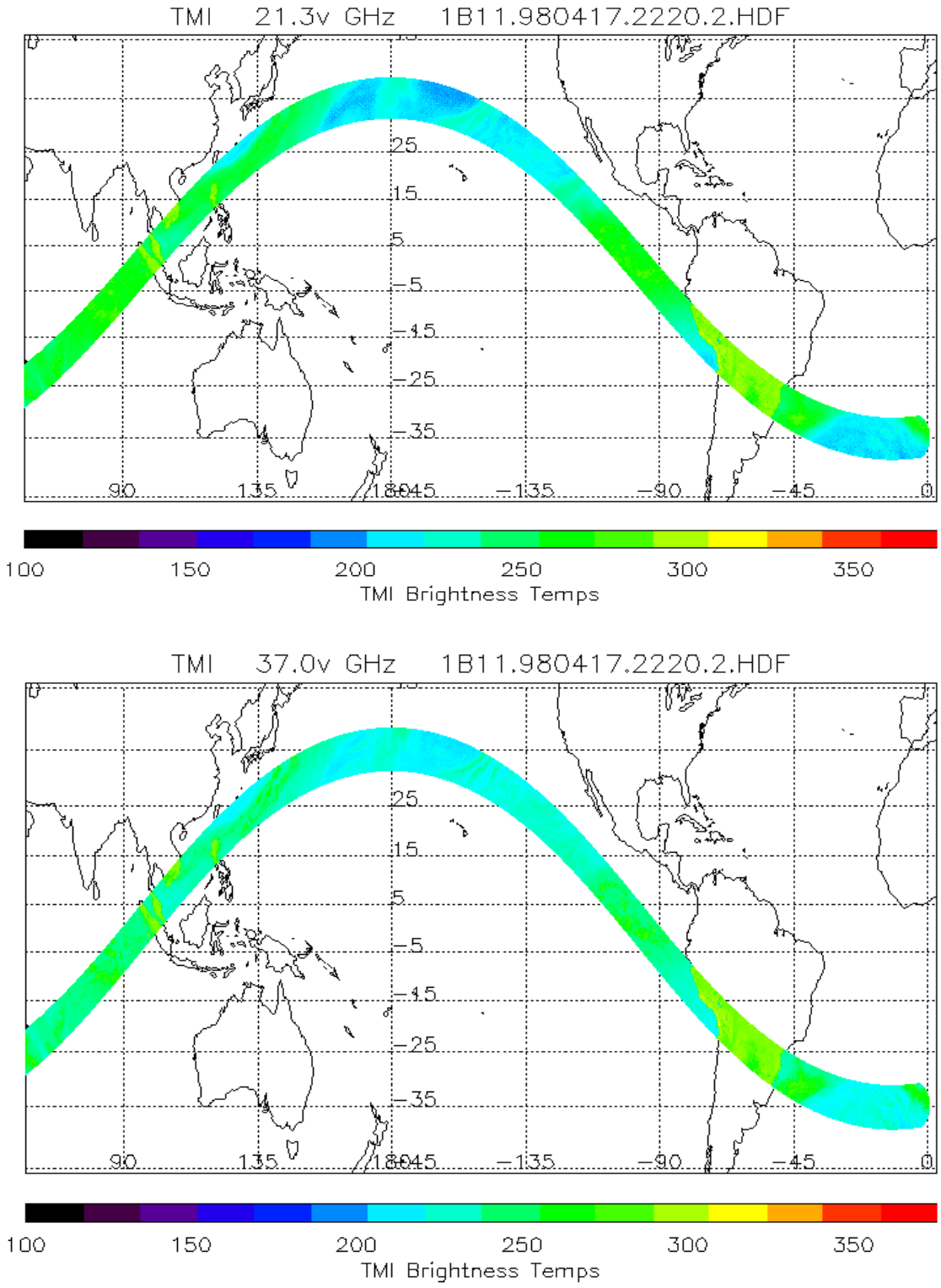

Fig. 4.1 Continued. b) One orbit of TMI 1B11 BT data for 21v, and 37v GHz

4.3.2 New Temperature Profile

The TAMU algorithm based on Wilheit et al. (1977) algorithm has assumed the temperature profile in the RTM using the lowest section of the U.S. Standard Atmosphere where the lapse rate is 6.5 K/km. This is a typical value from sea level to 10 or 15 km altitude. It is not necessarily typical of raining conditions.

A new lapse rate is assumed to be 5.3 K/km below the FL and to be 6.5 K/km above the FL. It is justified by the observations in the tropics. This introduces a different lapse rate, closer to the moist adiabatic lapse rate than lapse rate in the U.S standard atmosphere. Above the FL, the old 6.5 K/km, lapse rate was retained. Figure 4.2 describes a new temperature profile in the current TAMU RTM.

4.3.3 Procedures for the Comparison

Firstly, for the PR FL retrieval, individual pixels classified as stratiform are found using the definition of the BBH and the mirror image using PR data. The nadir direction is selected to detect the existence of bright band (BB) and the mirror images that are features of FLs. The detection of the BB and FL is made by a spatial filter, which is based on the first derivative of the returned power (dBm) with respective to range, and by imposing several conditions on the BB and FL as follows.

(1) The power above the BB peak should decrease appreciably.

(2) The power below the mirror image should decrease appreciably.

(3) The FL is the location of the steepest slope with respect to height above the peak of BB.

(4) The largest peak value indicates the surface.

(5) The distance between the surface and the BBH should be equal to the distance between the surface and the mirror image.

(6) After looking for stratiform rain cases automatically, all the cases are manually inspected to determine whether or not they are acceptable as stratiform rain cases.

(7) When the above conditions are satisfied, the rain type can be classified as stratiform rain.

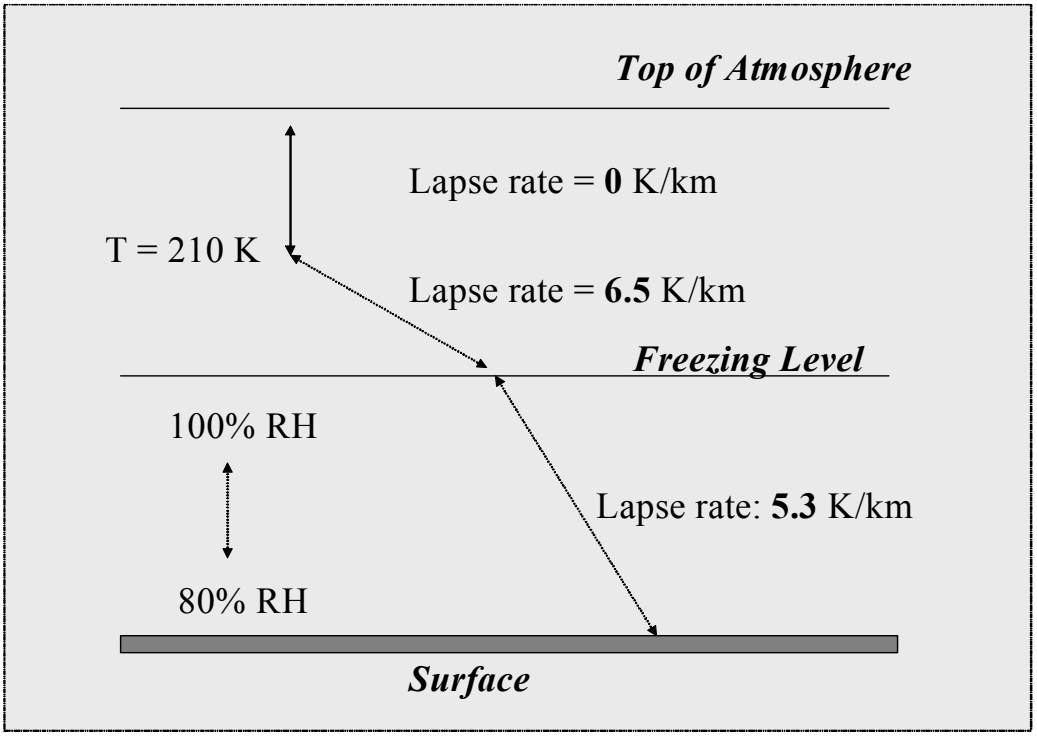

Fig. 4.2 New assumption of temperature profile

Secondly, matching TMI measurements with PR observations spatially and temporally is individually implemented using the latitude, longitude, time information of each pixel. Next, The TMI BTs are used as input parameters to retrieve the TMI FLs using a lookup table.

Thirdly, the two retrieved FLs are compared. Figure 4.3 shows an example of TMI FL, PR FL, and corresponding BTs of 19v and 21v channels.

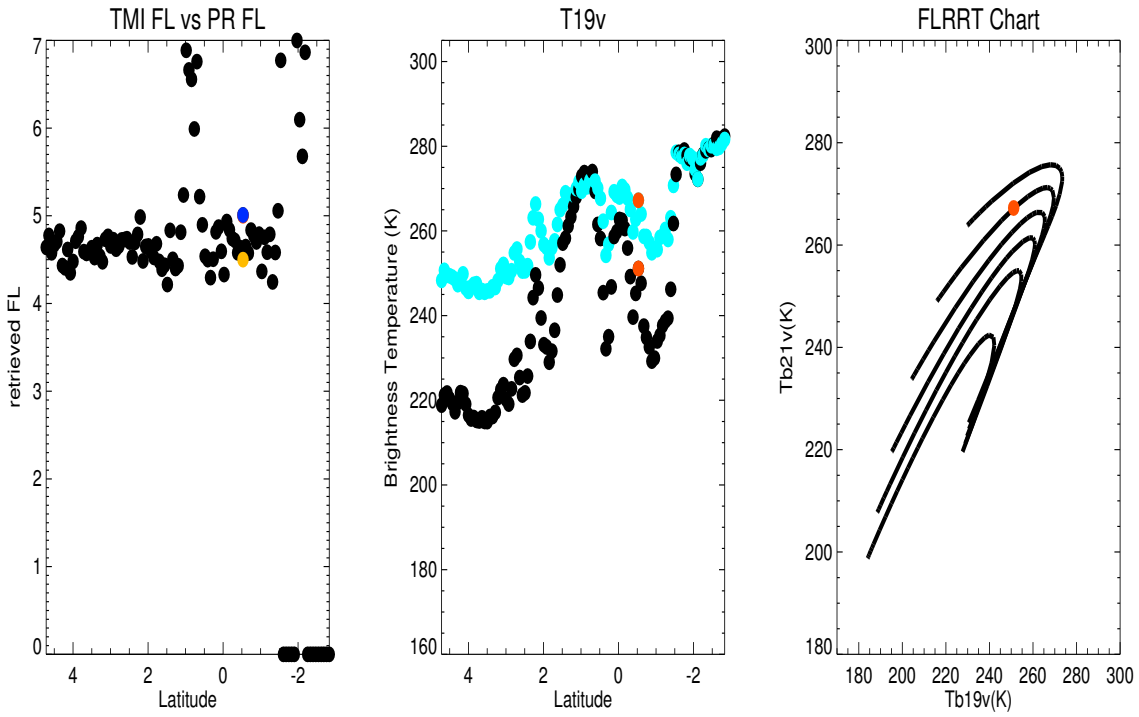

Fig. 4.3 Each panel depicts, respectively, an example of the TMI FL (black and blue circles) and PR FL (orange), BTs of 19GHz (black) and 21GHz (sky-blue) channels, and the FLRRT chart when TMI and PR observations coincide over the ocean

4.4 Results

The total number of coincident BB, and mirror images is 544 cases. Those are used for the comparison to investigate the effect of a new temperature profile on the FL retrieval. The difference among the mean values of the PR FL (a), the BBH, (b) and the TMI FL using the current lapse rate (c), and new lapse rate (d) are as follows:

(a) is 0.44 km higher than (b).

(a) is 0.44 km higher than (d).

(c) is 0.73 km lower than (a).

The mean difference between the PR FL and the BBH is 459m during Dec. 1997, 445m during Jan. 1998, 444m during Dec. 1999, and 446m during Jan. 2000. The mean difference between the PR FL and the BBH is slightly higher in the El Niño (1997 ~ 1998) than in the normal years (1999 ~ 2000) when we use previous results. The averaged difference indicated that the BBH occurs at heights ranging from 440~460m below the PR FL. From Figure 4.4, it occurs at heights from 250m~1000m below the FL. The following comparisons show the monthly averaged differences among the values.

For the Dec. 1997,

(a) is 0.459 km higher than (b).

(a) is 0.517 km higher than (d).

(c) is 0.812 km lower than (a).

For the Jan. 1998,

(a) is 0.445 km higher than (b).

(a) is 0.473 km higher than (d).

(c) is 0.728 km lower than (a).

For the Dec. 1999,

(a) is 0.444 km higher than (b).

(a) is 0.444 km higher than (d).

(c) is 0.745 km lower than (a).

For the Jan. 2000,

(a) is 0.446 km higher than (b).

(a) is 0.397 km higher than (d).

(c) is 0.674 km lower than (a).

From the results, TMI FL is still lower than PR FL but, the difference is reduced. The new temperature profile yields good agreement between the TMI FL and the BBH from PR observation. Figure 4.5 shows BBHs versus new TMI FLs.

Considering the vertical resolution of PR is 250m, the maximum uncertainty of PR FL is close to 250m. This indicates that the TMI FL is reasonable relative to the PR FL if the mean FL value is taken into account.

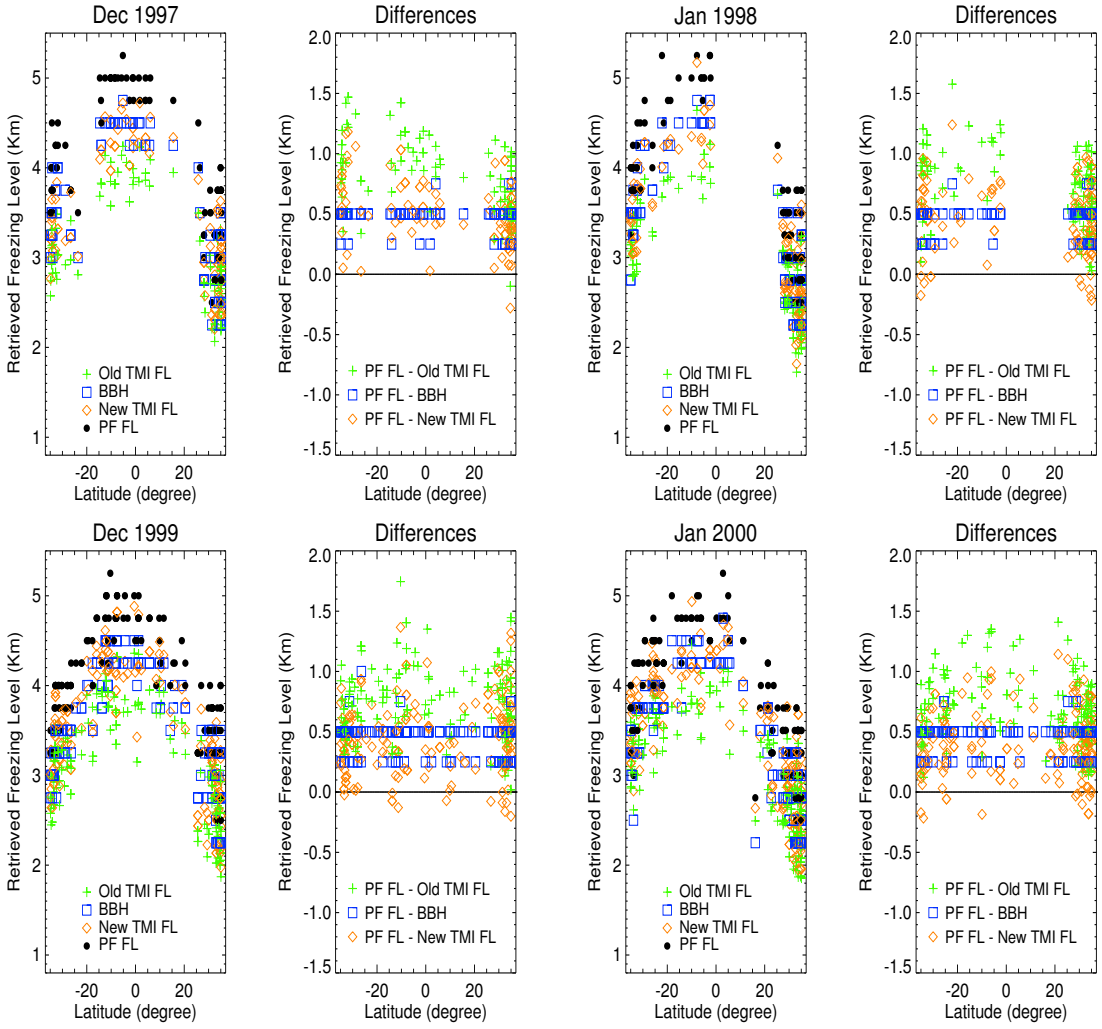

Fig. 4.4 Latitudinal distribution of PR FL, BBH, old TMI FL, and new TMI FL, latitudinal distribution of the differences among them

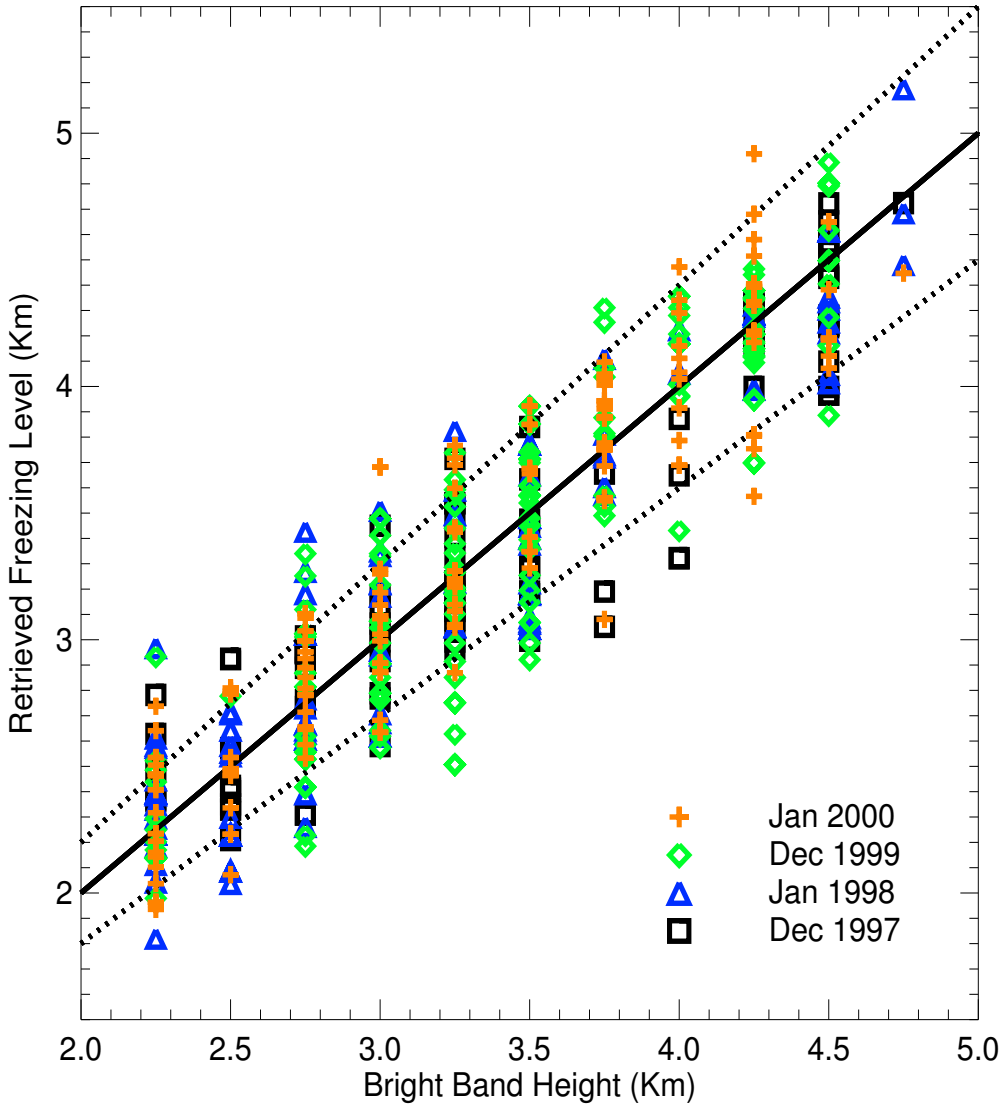

Fig. 4.5 BBH versus new FL. Each color represents data for different months. Dotted lines indicate 10% uncertainties between BBH and new FL

From these results, the old temperature profile is an error source to induce a large discrepancy between PR FL and TMI FL as previous works mentioned. Accordingly, there exists a large overestimation of the TMI-based rainfall retrieval. When the new temperature profile assumption is applied to the global FL retrieval using the TMI BTs as inputs, the new retrieved TMI FL agrees with the features of rainfall distribution in terms of the pattern because the uncertainty of FL is inversely proportional to the uncertainty of the rainfall. Figure 4.6 shows the global maps using the new TMI FL. Those figures show general features in El Niño and normal years.

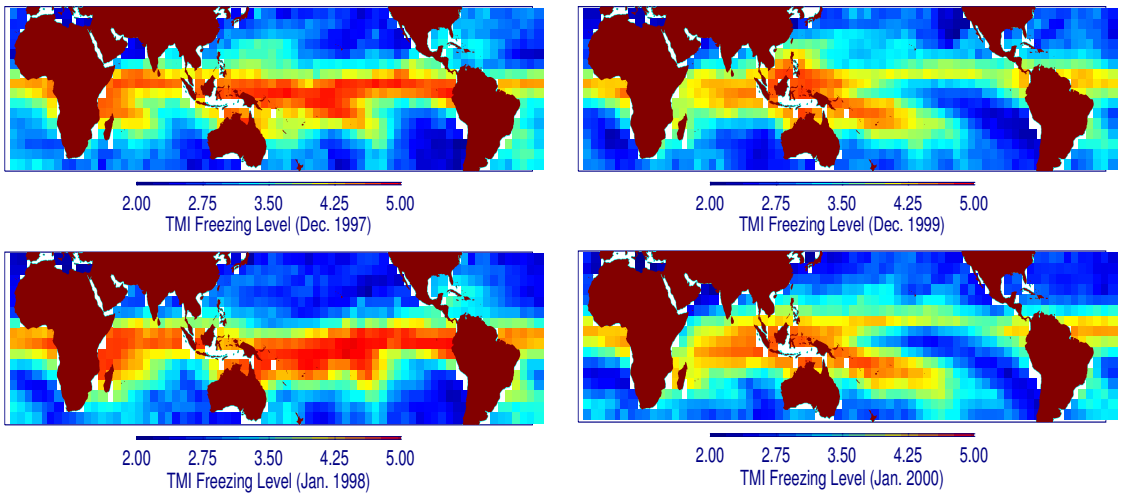

Fig. 4.6 Global map of the 5° × 5° averaged FL using the new temperature profile

The 5º latitude-averaged FL shows the expected seasonal characteristics. During the boreal winter, the retrieved TMI FL in the northern hemisphere is lower than in the southern hemisphere. El Niño periods show slightly higher TMI FLs than Normal years for the tropics. However, it is hard to find a difference between two periods for the higher latitudes.

4.5 Conclusion

A new temperature profile based on new observations results in an improved FL retrieval. The uncertainty of the TMI FL retrieval is reduced to within approximately 10%. This uncertainty is much smaller than the uncertainty due to the earlier thermodynamic assumptions. Accordingly, the uncertainty of rainfall estimation becomes smaller.

This new temperature profile assumption in the TAMU RTM can represent typical characteristics of tropics because it is based on observations in the tropics. This research emphasizes the role of the temperature profile on the BT calculation in the passive microwave algorithm. However, the FL uncertainty is relatively larger in the low FL region since the current TMI FL and PR FL have a low resolution as the FL becomes lower. If the temperature variability is small as in the tropics, the difference between the TMI FL and PR FL is very stable. Thus, a reasonable comparison can be made. This analysis can be extended to the Bayesian algorithm for microwave precipitation retrieval. Additional research on the low FL cases is required to understand the uncertainties of both FL and rainfall retrieval in the mid and high latitudes.

CHAPTER V

UNCERTAINTY OF RADIATIVE TRANSFER CALCULATION AMONG TEXAS A&M UNIVERSITY, EDDINGTON APPROXIMATION, DISCRETE ORDINATE, AND MONTE CARLO CODES

5.1 Previous Work

Kummerow (1993) compared an EDD and N-stream DO solution in the microwave regime through a plane parallel medium. He found the differences between an eight-stream DO solution and an analytical EDD solution ranged from 0 to 6 K when only one uniform layer of hydrometeors was considered. When realistic, multilayered cloud hydrometeor profiles were used, the differences between these two models never exeeded 3 K over the entire range of 6.6-183 GHz. The models agreed to within 0.2 K in the absence of scattering constituents. Roberti et al. (1994) compared 3-D DO, 3-D MC, and two different variations of plane parallel EDD methods. They found the discrepancies are rooted in numerical problems of the DO solution with additional noise in the ±1 K range being computed by the MC solution. Although the 3-D DO method has much better agreement with the MC results than plane parallel modeling gives, the maximum differences between two models can still be as large as 18.6 K for 85 GHz. Plane parallel results are warmer than 3-D calculations in heavy rain at low frequencies (10.7 and 19 GHz). Plane parallel result are generally colder than 3-D calculations at

high frequencies (37 and 85.6 GHz). Smith et al. (2002) compared microwave multiple scattering RT codes used in generating databases for satellite rainfall retrieval algorithms. Simulations were to be carried out for nadir and off-nadir (53.1º) observation angles at frequencies between 10 and 85 GHz. Among the RTM were two stream, multiple stream and MC models. They showed the largest discrepancies occurred at high frequencies where atmospheric scattering is most pronounced and at nadir observation. If the same surface boundary conditions, the same multiple-stream resolution and the same scaling procedures are used, the models were very close to each other with discrepancies below 1 K.

5.2 Methods

All codes were applied to the same TAMU RTM. View angles ranged from nadir to 80°. Rain rates were examined from 0.001 mm/hr to about 140 mm/hr. The FL was varied from 1 km to 5 km in 1km increments. Water vapor, oxygen gas, and cloud liquid water were included in the RTM. Ice layers were also assumed in some cases. Lambertian and specular surfaces were considered. 10, 19 and 37 GHz channels were tested.

For the DO code, the 16 stream case was considered. For the EDD, DO, and MC codes, the total asymmetry factors, total extinction coefficients, and total single scattering albedos in each layer were calculated from the TAMU RTM using Mie scattering.

For the MC code, the cloud is modeled with (2×2) horizontally finite and

vertically layered subclouds, surrounded by a background plane parallel atmosphere. Both the height and the number of the layers were assumed to be the same from subcloud to subcloud. The horizontal dimension of the subcloud was assumed to be 24 km×24 km. 3×3 points to compute the BT for each subcloud were located in each subcloud. 2×10^4 photons were used for the test in the MC code. This number of photons provides 0.71 % uncertainty. Figure 5.1 summarizes the TAMU RTM.

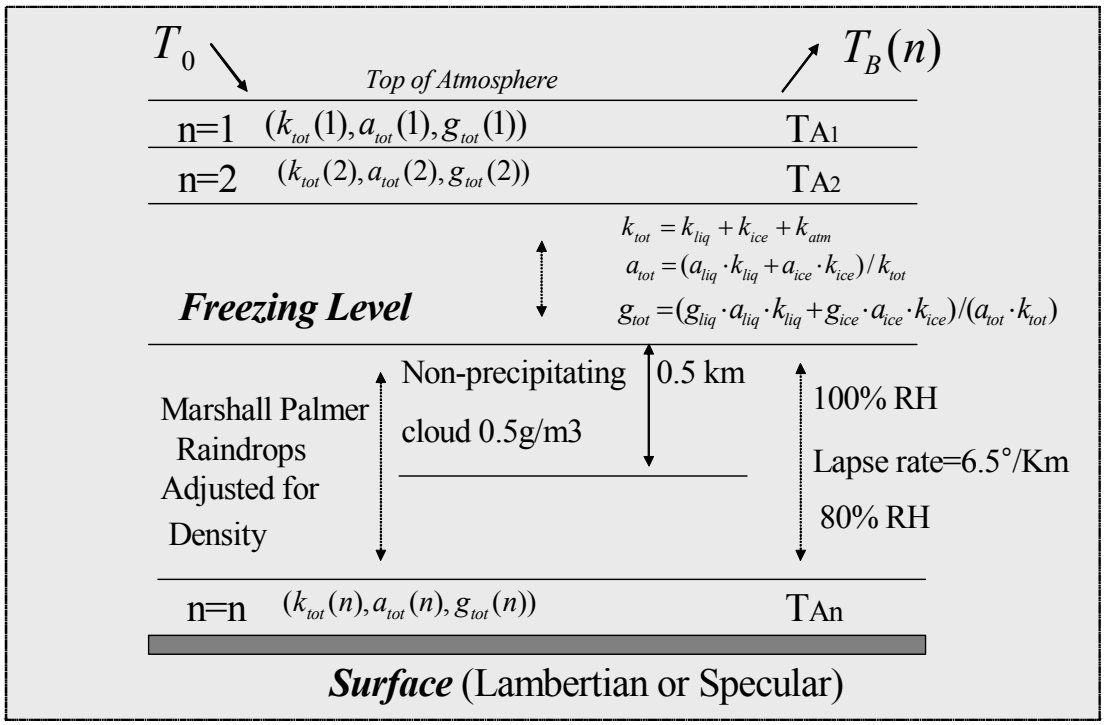

Fig. 5.1 TAMU RTM. g_{tot} **is total asymmetry factor.** a_{tot} **is total scattering albedo.** k_{tot} **is the total extinction coefficient**

5.3 Results

All RT codes show good agreement within the rain rate dynamic range of each channel at view angles from nadir to more than 60º but not near the limb. Generally, these codes show relatively large uncertainty of BTs pat the saturation point of each channel due to heavy rainfall. Figures 5.2 and 5.3 show the differences of the BTs among the codes for the Lambertian or specular surface, respectively. From the figures, the effect of ice layer on the BT is limited to heavy rainfall for each channel.

To investigate the impact of RT codes on the retrieval of FLs, the previously discussed TMI data (Dec. 1997, Jan. 1998, Dec.1999, and Jan. 2000) are utilized. 546 cases, where BBs and mirror images coexist simultaneously, are used for the comparison among TAMU FL, EDD FL, DO FL and MC FL. Low FLs, below 2 km, have large uncertainty in both TMI and PR. If only FLs over 2 km are considered, and FLRRT charts are made for the current sensor view angle (53º) using the TAMU, EDD, DO, and MC codes, the uncertainties of the FLs due to the BTs among the RT codes can be estimated. The difference among the mean value of PR FL (a), BBH (b), TAMU FL (c), EDD FL (d), DO FL (e), and MC FL (f) are summarized in Table 5.1. The mean differences between FLs and BBH for each month are are summarized in Table 5.2.

Table 5.1 The difference among the mean value of PR FL (a), BBH (b), TAMU FL (c), EDD FL (d), DO FL (e), and MC FL (f)

	(a) - (b)	(a) - (c)	(a) - (d)	(a) – (e)	(a) - (f)
Difference (km)	0.44	0.45	0.48	0.17	0.62

Table 5.2 The mean differences between FLs and BBH for each month

Difference (km)	(b) - (c)	(b) - (d)	(b) - (e)
Dec. 1997	0.06	0.10	0.25
Jan. 1998	0.03	0.07	0.23
Dec. 1999	0.00	0.04	0.18
Jan. 2000	-0.05	-0.02	0.09

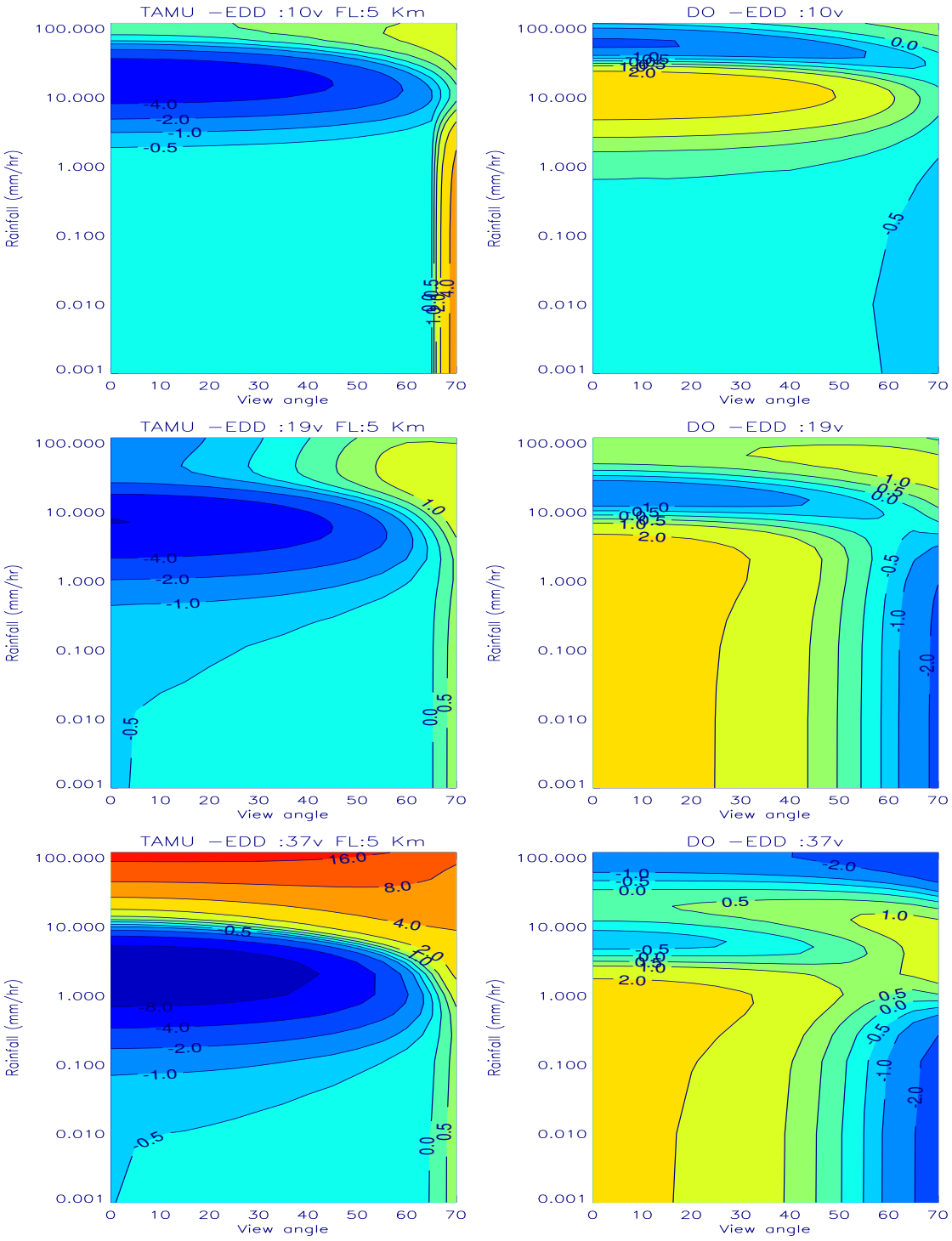

Fig. 5.2 Contour of BT differences using TAMU, EDD, and DO codes for the Lambertian surface, respectively. The FL is assumed to be 5 km

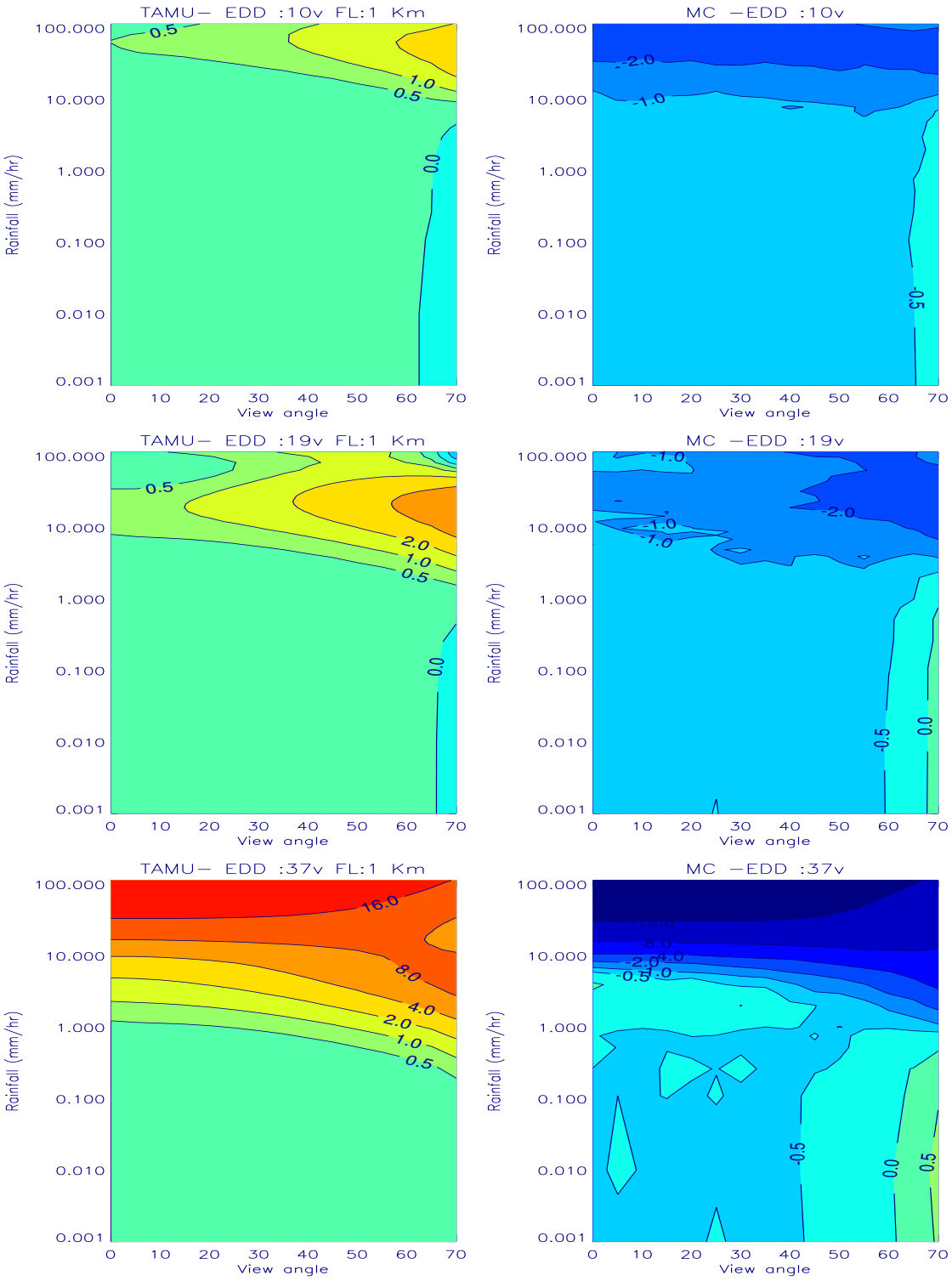

Fig. 5.3 Contour of BT differences using TAMU, EDD, and MC codes for the specular surface, respectively. The FL is assumed to be 1 km

From the results, the TAMU FLs are almost the same as the EDD FLs but, the EDD FLs are slightly lower than TAMU FLs. The MC FLs are, on average, 180m lower than BBH. This value is still within the reasonable uncertainty of the BBH because the vertical resolution of the PR is 250 m.

Figure 5.4 shows the BT differences among the RT codes used to retrieve the FLs and rain rates. For 3, 4, and 5 km FLs, the TAMU code and EDD code agree to better than 1 K. The TAMU code and DO code agree from 1 K to 3 K. The TAMU code and MC code agree from 1 K to 3.5 K. Figure 5.5 depicts a) Latitude vs. FL differences, b) 19 GHz vertical channel's BT vs. FL differences, c) latitude vs. BBH-FLs. In those cases, FLs are retrieved from the FL lookup tables using TAMU, EDD, and MC codes. The BTs observed during Dec. 1997, Jan. 1998, Dec.1999, and Jan. 2000 are used as input data to validate the FLs. Figure 5.6 shows a) the relationship between the latitude and FL differences among TAMU FL, EDD FL, and MC FL and b) the relationship between the latitude and BBH-FLs for Dec. 1997, Jan. 1998, Dec.1999, and Jan. 2000 respectively. In Figure 5.7, FL differences vs. rain rates among TAMU FL, EDD FL, DO FL are shown using BTs generated from TAMU code. In this case, FLs are retrieved from their own FL lookup table. Figure 5.8 describes the FL differences vs. rain rates among TAMU FL, EDD FL, and DO FL retrieved using the TAMU FL lookup table BTs.

Collectively, the BT differences are less than 3 K among the 4 RT codes within the range of the physical FL and rain rate retrievals. The relatively large discrepancies of BTs among the RT codes occur at high latitude, high BTs, low FLs and heavy rainfall. Those are caused by different approaches to solving the scattering term in the RTE.

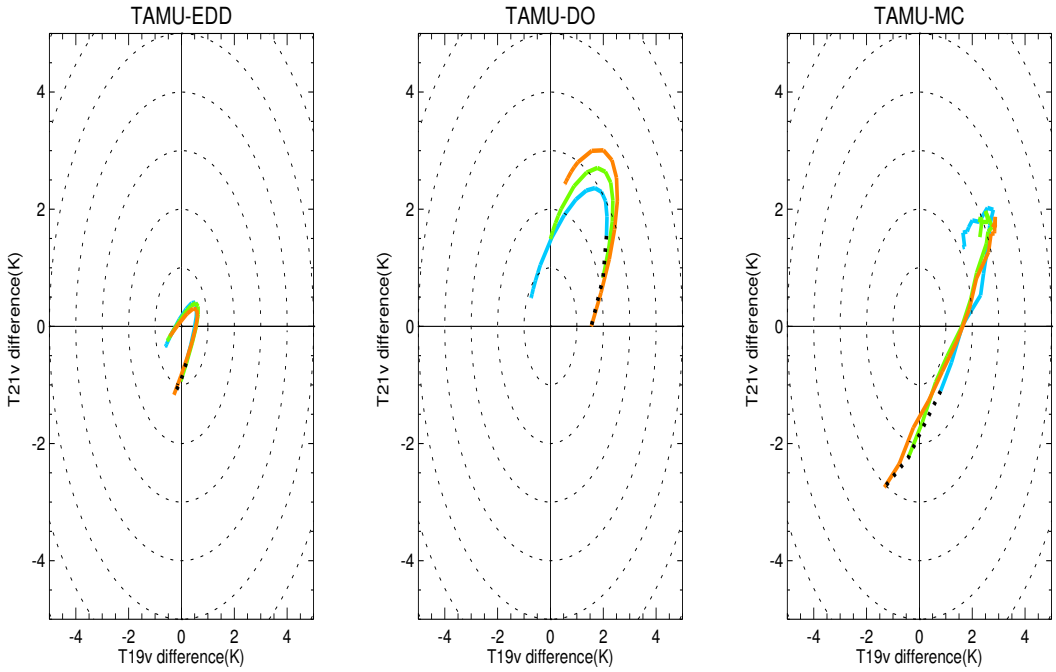

Fig. 5.4 BT differences among the RT codes to retrieve the FLs and rain rates

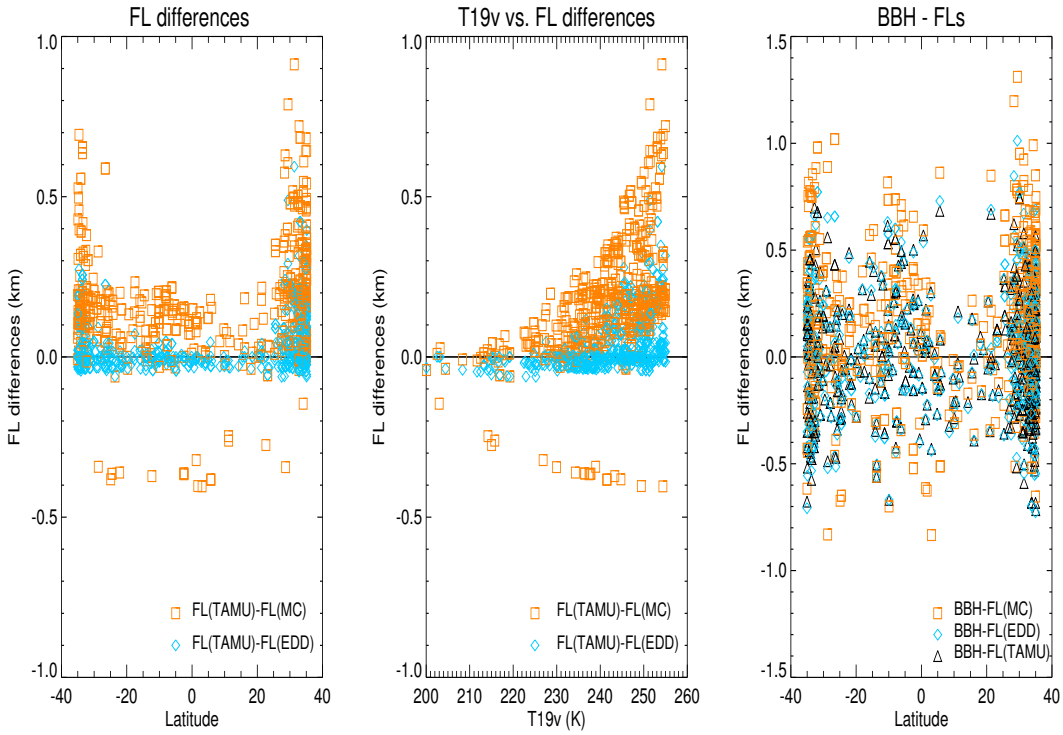

Fig. 5.5 a) Latitude vs. FL differences. b) 19 GHz vertical channel's BTs vs. FL differences c) Latitude vs. BBH-FLs. In those cases, FLs are retrieved from the FL lookup tables using TAMU, EDD, and MC codes. The BTs observed during Dec. 1997, Jan. 1998, Dec.1999, and Jan. 2000 are used as input data to validate the FLs

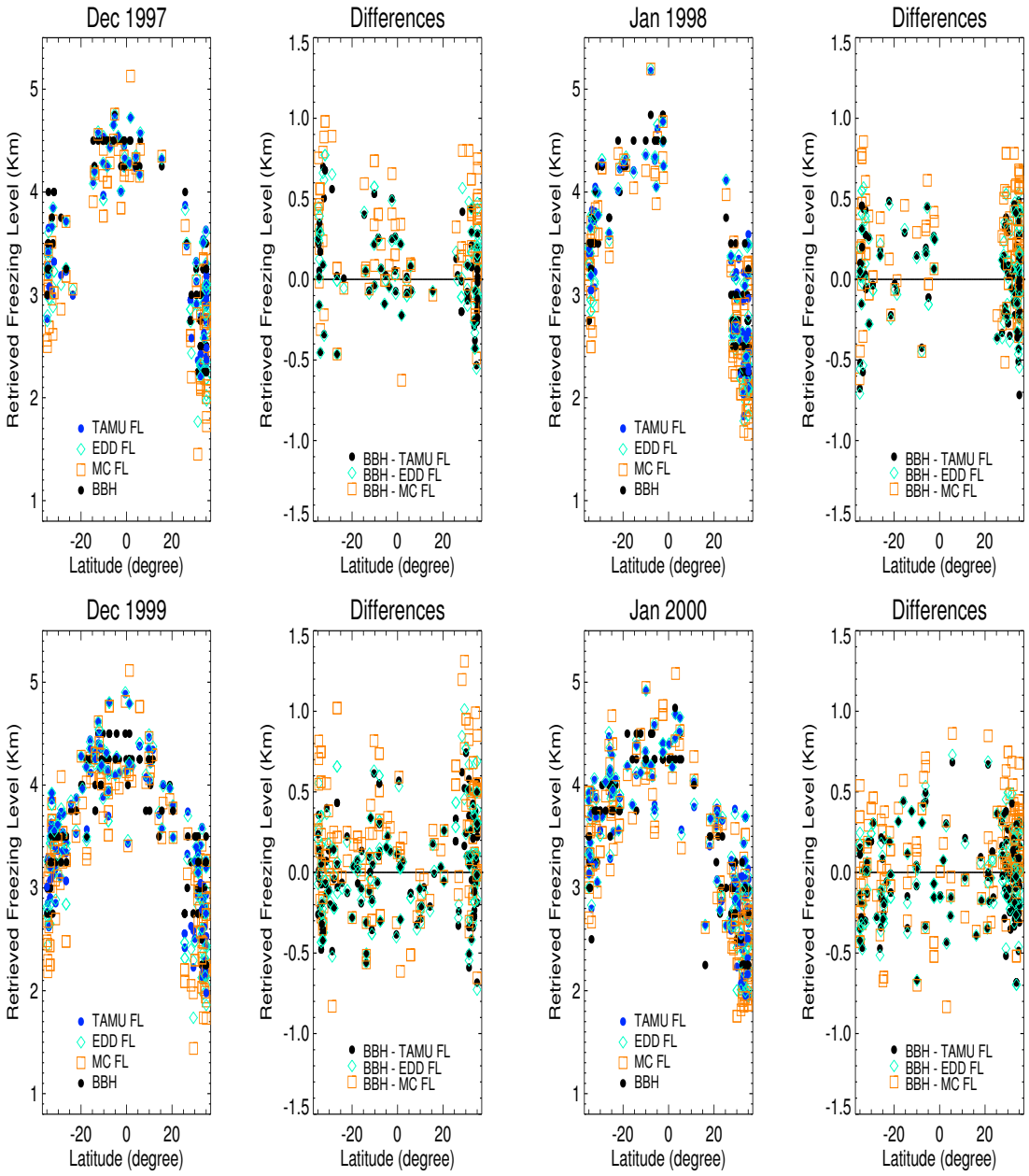

Fig. 5.6 Latitude vs. FL differences (TAMU FL, EDD FL, and MC FL) and latitude vs. BBH-FLs for Dec. 1997, Jan. 1998, Dec.1999, and Jan. 2000 respectively

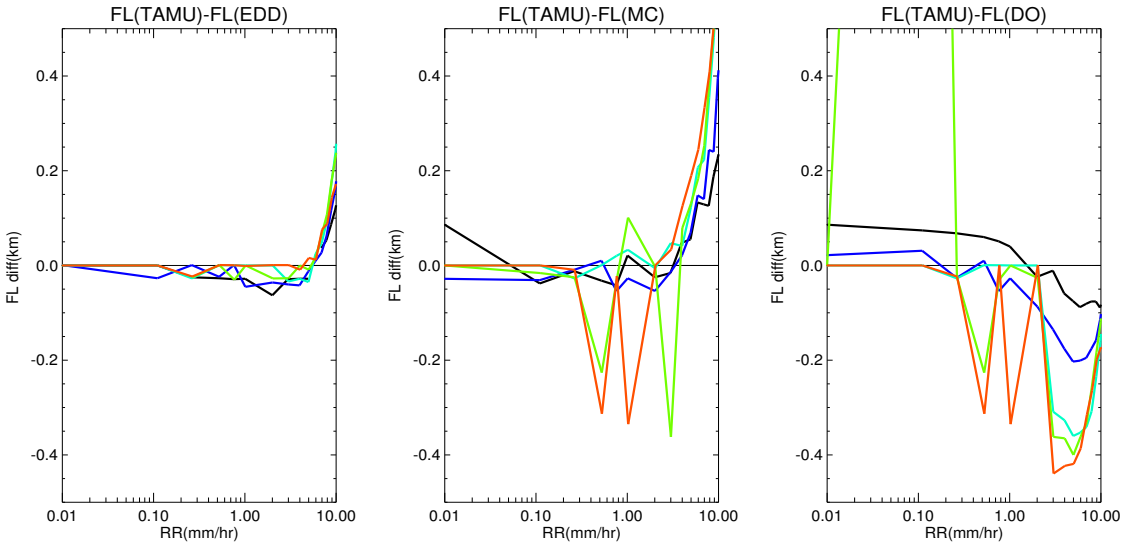

Fig. 5.7 FL differences vs. rain rates among TAMU FL, EDD FL, DO FL using BTs generated from TAMU code. In this case, FLs are retrieved from their own FL lookup table

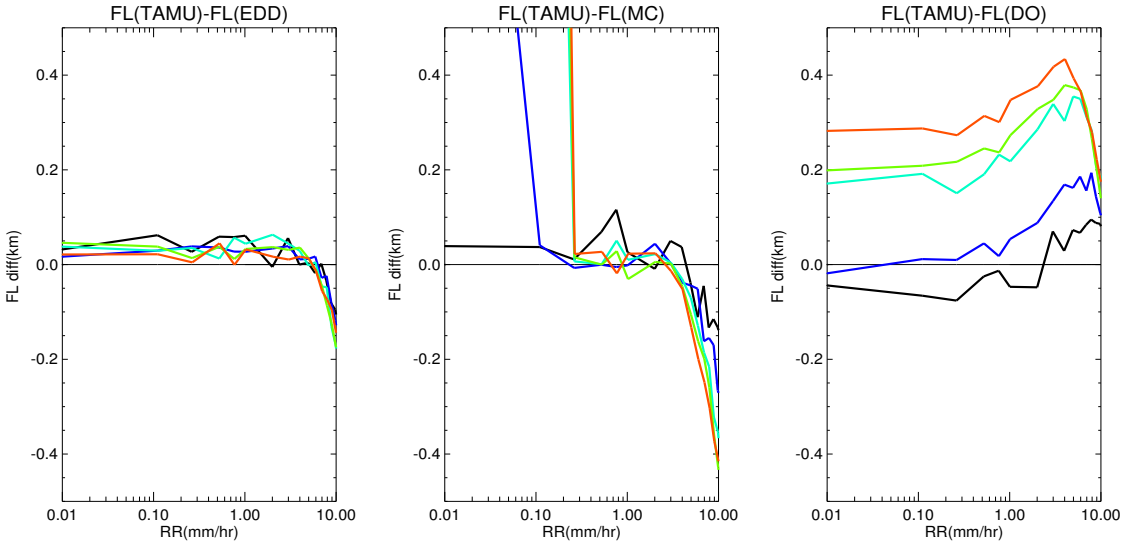

Fig. 5.8 FL differences vs. rain rates among TAMU FL, EDD FL, DO FL using BTs generated from each code. In this case, FLs are retrieved from only TAMU FL lookup table

5.4 Conclusion

The BT differences between the TAMU code and the EDD code are less than 0.5 K for the 10v, 19v, and 37 GHz channels and various FLs at all view angles, except near the limb irrespective of the surface properties. The BTs between the EDD and DO codes differ by less than 1 K for the 10v, 19v, and 37 GHz channels and all FLs at the current sensor view angle (53º) with the Lambertian surface. This result agrees with the description in the previous work done by Kummerow (1993). At the nadir and limb, BT discrepancies are around 2 K. The EDD and MC codes for the specular surface agree with each other less than 1 K for the 10v, 19v, and 37 GHz channels and low FLs, Otherwise, the BT difference between two codes increases up to 4 K as the FL increases. This result indicates the plane parallel results are warmer in heavy rain than MC calculations at 19 and 37 GHz, but the plane parallel results are colder than MC calculations at 10 GHz. Plane parallel results are generally colder than MC calculations at most rain rates through the whloe range of view angle irrespective of the FLs. This analysis agrees quite well with the previous work.

For the FLs and rainfall retrieval in the tropics, 4 RT codes can lead to the similar results because the BT differences among the RT codes are less than 3 K at the 3-5 km FLs. The selection of the RT codes should be considered due to various view angles in the GPM. From this research, the TAMU, EDD, and MC codes show good agreement through the whole range of view angles within the rain rate dynamic range of each channel. The BT differences among 4 RT codes are relatively large past saturation point of each channel.

The uncertainties of BTs among the TAMU, EDD, DO, and MC codes at the low FLs should be studied in the future because the BT differences among the RT codes increase as the FL decreases.

5.5 Future Work

For future work, ice thickness can be another parameter used to retrieve heavy rainfall using a combination of 10 GHz and 37 GHz. BTs. By combination of active and passive microwave algorithms, the FL can be determined. Since current passive FL retrieval scheme using FLRRT chart can not determine if or not the rainfall is heavy, a combination of two FL retrieval methods will be useful. After the FL is determined, the ice thickness can be estimated using ice thickness lookup tables. In this case, various BTs will be also used as input data. Irrespective of the RT codes, the pattern of relationships between rain rate and BTs appear similar in the limit of heavy rainfall. Figure 5.9 show the behavior of each channel's BTs with respect to the ice thickness varied from 0 to 12 km using TAMU, EDD, and DO codes.

This generates an opportunity to retrieve the FL and ice thickness in middle and high latitudes using current channels.

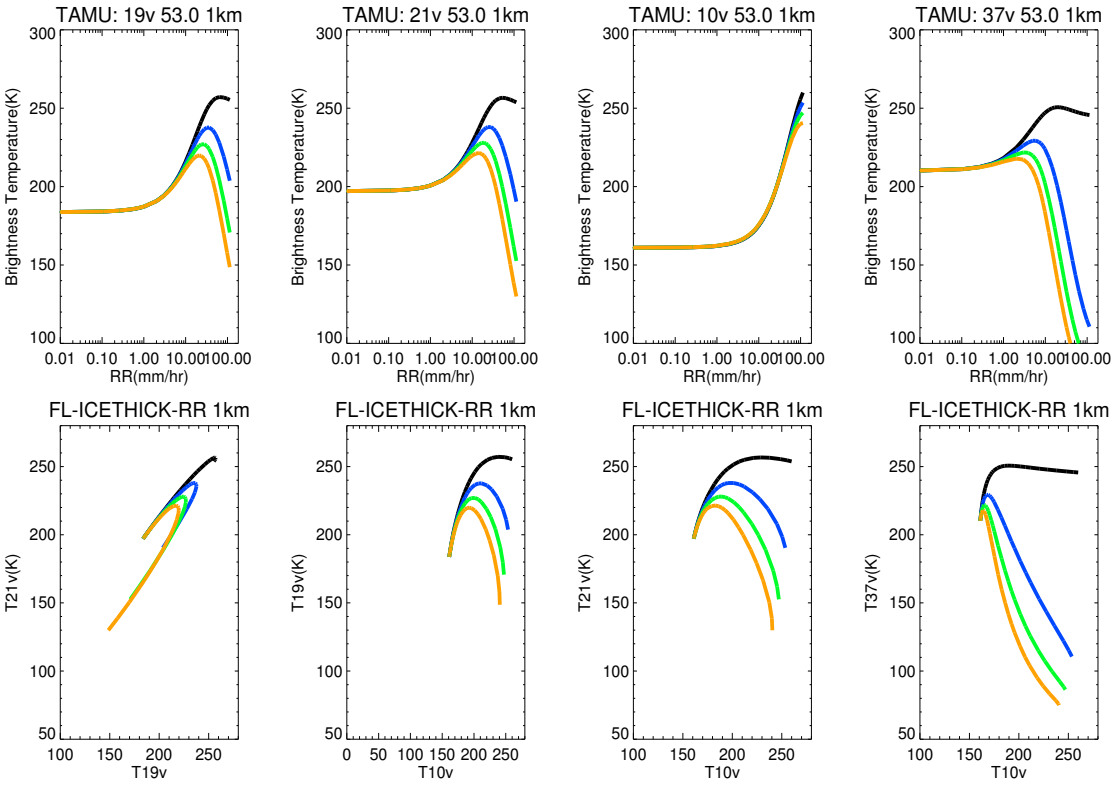

Fig. 5.9 Rain rates vs. BTs. Each color describes the different ice thickness from 0 to 12 km over the FL. And the combination of 10, 19, 21, and 37 GHz channel's BTs. a) TAMU code

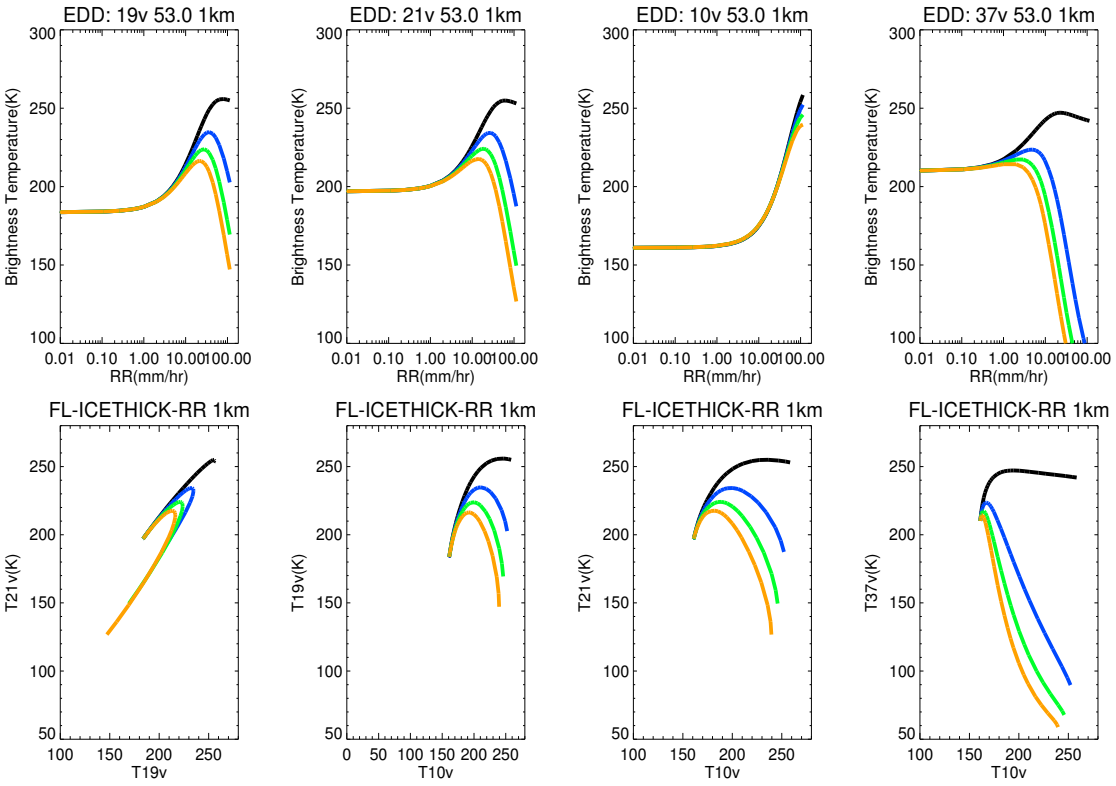

Fig. 5.9 Continued. b) EDD code

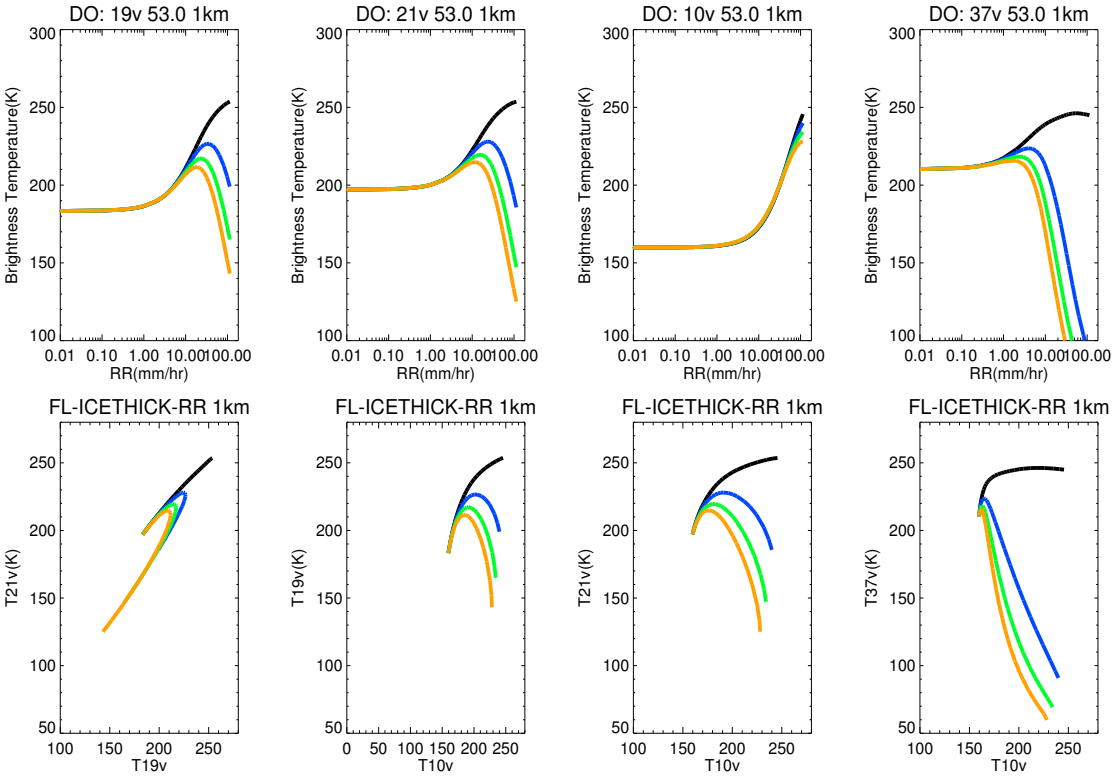

Fig. 5.9 Continued. c) DO code

CHAPTER VI

CONCLUSION AND SUMMARY

6.1 Effects of Vertical Resolution on Brightness Temperature

The effect of vertical resolution in the RT algorithm on the computational efficiency and uncertainty through the inter-comparison among the TAMU and EDD codes was researched. The very light rainfall case was considered for the effect of vertical resolution on the BTs. The assumed number of layers (vertical resolution) in the passive microwave RT codes lead to slightly different BTs even if the same RTM is used. The uncertainty of the BT from the vertical resolution decreases as the assumed number of layers increases. Fewer layers are needed to obtain the same uncertainty ($\leq$ 0.5 K) for both codes for the Lambertian surface than the specular surface. Those vertical resolutions are approximately half or double the value of the PR resolution, respectively.

The uncertainties are due to the optical thickness because the layer optical thickness is a function of the vertical resolution. This research is the first useful trial to determine the effect of vertical resolution in the RTM.

6.2 Improved Freezing Level Retrieval in Oceanic Rainfall Algorithm

The uncertainty of the TMI FL retrieval is reduced to within approximately 10% when a new temperature profile based on new observations is used in the FL retrieval. The result of this research emphasizes the role of the temperature profile on the BT calculation in the passive microwave algorithm. However, the FL uncertainty is

relatively larger in the low FL region since the current TMI FL and PR FL have a low resolution as the FL becomes lower. Accordingly, additional research on the low FL cases is required to understand the uncertainties of both FL and rainfall retrieval in the mid and high latitudes.

6.3 Uncertainty of Radiative Transfer Calculation among Texas A&M University, Eddington Approximation, Discrete Ordinate, and Monte Carlo Codes

The TAMU, EDD, and MC codes show good agreement through the whole range of view angles within the rain rate dynamic range of each channel. The BT differences among 4 RT codes are relatively large past saturation point of each channel. For the FLs and rainfall retrieval in the tropics, 4 RT codes can lead to the similar results because the BT differences among the RT codes are less than 3 K at the 3-5 km FLs. The selection of the RT codes should be considered due to various view angles in the GPM. The uncertainties of BTs among the TAMU, EDD, DO, and MC codes at the low FLs should be studied in the future because the BT differences among the RT codes increase as the FL decreases.

6.4 Future Work

Ice thickness can be another parameter used to retrieve heavy rainfall using a combination of 10 GHz and 37 GHz. BTs with the FL retrieval based on the combination of active and passive microwave algorithms. This will generate an opportunity to retrieve both the FL and ice thickness in middle and high latitudes using current channels.

REFERENCES

Berg, W., C. Kummerow, and C. A. Morales, 2002: Differences between East and West Pacific rainfall systems. *J. Climate,* **15,** 3659–3672.

Chiu, L. S., and A. T. C. Chang, 2000: Oceanic rain column height derived from SSM/I. *J. Climate,* **13,** 4125–4136.

Gunn, K.L.S. and T.U.R. East, 1954: The microwave properties of precipitation particles. *Quart. J.Roy. Meteor. Soc.* **80**, 522-545.

Ikai, J., and K. Nakamura, 2003: Comparison of rain rates over the ocean derived from TRMM microwave imager and precipitation radar. *J. Atmos. Oceanic Technol,* **20**, 1709–1726.

Kummerow, C., and J. A. Weinman, 1988: Determining microwave brightness temperatures from the horizontally finite, vertically structured cloud*, J. Geophys. Res.***,** **93**, 3720-3728.

Kummerow, C., 1993: On the accuracy of the Eddington approximation for radiative transfer in the microwave frequencies, *J. Geophys. Res.,* **98**, 2757-2765.

Lane, J.A., and J. A. Saxton, 1952: Dielectric dispersion in pure polar liquids at very high radio frequencies*. Proc. Roy. Soc. London*, A**214**, 531-545.

Liou, K., 1992: *Radiation and cloud processes in the atmosphere*, Oxford University Press, 487pp.

Rangno, A. L and P.V. Hobbs, 2005: Microstructures and precipitation development in cumulus and small cumulonimbus clouds over the warm pool of the tropical Pacific Ocean. *Quart. J. Roy. Meteor. Soc.,* **131**, 639-673.

Roberti, L., J. Haferman, and C. Kummerow, 1994: Microwave radiative transfer through horizontally inhomogeneous precipitating clouds, *J.Geophys. Res*., **99**, 16,707–16,718.

Rosenkranz, P. W., 1993: Absorption of microwaves by atmospheric gases. *Atmospheric Remote Sensing by Microwave Radiometry*, M. A. Jansen, Ed., Wiley Series in Remote Sensing, John Wiley & Sons, Inc., 37-90.

Rosenkranz, P. W., 1998: Water vapor microwave continuum absorption: A comparison of measurements and models. *Radio. Sci*., **33**(4): 919-928.

Smith, E. A., P. Bauer, F. S. Marzano, C. D. Kummerow, D. McKague, A. Mugnai, and G. Panegrossi, 2002: Intercomparison of microwave radiative transfer models for precipitating clouds, *IEEE Trans. on Geosci. and Remote Sens.*, **40**, 541-549.

Stamnes, K., S.-C. Tsay, W. Wiscombe, and K. Jayaweera, 1988: Numerically stable algorithm for discrete-ordinate-method radiative transfer in multiple scattering and emitting layered media, *Applied Optics*, **27**, 2502-2509.

Thurai, M., E. Deguchi, T. Iguchi, and K. Okamoto, 2003: Freezing height distribution in the tropics, *Int. J. Satell. Commun. Network*, **21**, 533-545.

Weinman, J. A., and R. Davies, 1978: Thermal microwave radiances from horizontally finite clouds of hydrometeors, *J.Geophys. Res.,* **83**, 3099-3107.

Wilheit, T. T., A. Chang, M. Rao, E. Rogers, and J. Theon, 1977: A satellite technique for quantitatively mapping rainfall rates over ocean, *J. Appl. Meteor.,* **16**, 551-560.

Wilheit, T. T., A. Chang, and L. Chiu, 1991: Retrieval of monthly rainfall indices from microwave radiometric measurements using probability distribution functions. *J. Atmos. Oceanic Technol.,* **8**, 118–136.

Wilheit, T. T., R. Adler, S. Avery, E. Barrett, P. Bauer, W. Berg, A. Chang, J. Ferriday, N. Grody, S. Goodman, C. Kidd, D. Kniveton, C. Kummerow, A. Mugnai, W. Olson, G. Petty, A. Shibata, E. Smith, and R. Spencer, 1994: Algorithms for the Retrieval of Rainfall from Passive Microwave Measurements, *Reviews of Remote Sensing* **11**, 163-194.

VITA

Sung Wook Hong was born in Seoul, Korea on August 26, 1971. He earned his Bachelor of Science degree in earth sciences in February, 1997, and then a Master of Science degree in physics in February, 2000 both from Seoul National University in Korea. He entered the Master of Science program in the Department of Atmospheric Sciences at Texas A&M University, and became a member of the Microwave Remote Sensing Group in the fall of 2001. He earned a Master of Science degree in December 2002 and a Doctor of Philosophy degree in August 2006, both in atmospheric sciences. He will work as a research scientist for NESDIS at NOAA in Camp Springs, Maryland from Octorber, 2006. Correspondence may be addressed to a continuing email at *sesttiya@gmail.com*, or U.S. mail, sensor physics branch, NOAA/NESDIS/STAR 5200 Auth Rd, Camp Springs, MD 20746.